

AD-A187 345

AD

12

DTIC FILE COPY

TECHNICAL REPORT BRL-TR-2828

A NUMERICAL ALGORITHM FOR THE  
MULTIDIMENSIONAL, MULTIPHASE  
VISCIOUS EQUATIONS OF  
INTERIOR BALLISTICS

JAMES A. SCHMITT

JULY 1987

DTIC  
ELECTE  
NOV 06 1987  
S D

APPROVED FOR PUBLIC RELEASE, DISTRIBUTION UNLIMITED

US ARMY BALLISTIC RESEARCH LABORATORY  
ABERDEEN PROVING GROUND, MARYLAND

Destroy this report when it is no longer needed.  
Do not return it to the originator.

Additional copies of this report may be obtained  
from the National Technical Information Service,  
U. S. Department of Commerce, Springfield, Virginia  
22161.

The findings in this report are not to be construed as an official  
Department of the Army position, unless so designated by other  
authorized documents.

The use of trade names or manufacturers' names in this report  
does not constitute indorsement of any commercial product.

UNCLASSIFIED

SECURITY CLASSIFICATION OF THIS PAGE

Form Approved  
OMB No 0704-0188  
Exp Date Jun 30, 1986

## REPORT DOCUMENTATION PAGE

1a REPORT SECURITY CLASSIFICATION Unclassified			1b RESTRICTIVE MARKINGS		
2a SECURITY CLASSIFICATION AUTHORITY			3 DISTRIBUTION/AVAILABILITY OF REPORT		
2b. DECLASSIFICATION/DOWNGRADING SCHEDULE					
4. PERFORMING ORGANIZATION REPORT NUMBER(S)  BRL-TR-2828			5 MONITORING ORGANIZATION REPORT NUMBER(S)		
6a. NAME OF PERFORMING ORGANIZATION  Ballistic Research Laboratory		6b OFFICE SYMBOL (If applicable)  SLCBR-IB-A	7a NAME OF MONITORING ORGANIZATION		
6c. ADDRESS (City, State, and ZIP Code)  Aberdeen Proving Ground, MD 21005-5066			7b ADDRESS (City, State, and ZIP Code)		
8a. NAME OF FUNDING/SPONSORING ORGANIZATION		8b OFFICE SYMBOL (If applicable)	9 PROCUREMENT INSTRUMENT IDENTIFICATION NUMBER		
8c. ADDRESS (City, State, and ZIP Code)			10 SOURCE OF FUNDING NUMBERS		
			PROGRAM ELEMENT NO. 61102A	PROJECT NO 1L161102AH43	TASK NO 00
			WORK UNIT ACCESSION NO 00		
11 TITLE (Include Security Classification)  A Numerical Algorithm for the Multidimensional, Multiphase, Viscous Equations of Interior Ballistics					
12. PERSONAL AUTHOR(S) James A. Schmitt					
13a TYPE OF REPORT Technical Report		13b TIME COVERED FROM Jan 81 TO Jan 83		14 DATE OF REPORT (Year, Month, Day)	15 PAGE COUNT
16. SUPPLEMENTARY NOTATION					
17 COSATI CODES			18 SUBJECT TERMS (Continue on reverse if necessary and identify by block number)  Alternating Direction Implicit, DELTA		
FIELD	GROUP	SUB-GROUP			
19	01				
21	02				
19 ABSTRACT (Continue on reverse if necessary and identify by block number) A numerical method based on a linearized ADI (Alternating Direction Implicit) scheme is described in the context of the solution procedure for the nonlinear partial differential equations associated with an average two-phase (gas-solid), two-dimensional, fully viscous model of interior ballistics. This method was chosen because the linearization of the time-differenced equations within the temporal truncation error permits a non-iterative solution procedure for this implicit scheme, and the splitting of difference equations along the coordinate directions provides a block tridiagonal structure of the solution matrices. The implementation of the algorithm possesses several novel features: the algorithm is derived in the context of a moving coordinate system; the non-conservational form of the governing equations avoids both mass sources (which can be generated by grid motion) and singular solution matrices (which can arise in regions of one-phase flow in a two-phase calculation); and finally, the Jacobian type matrices (which arise from the linearization process) are determined by numerical differentiation instead of the usual analytic calculations. This numerical scheme is encoded in the DELTA computer code. ⚡					
Verification of the DELTA algorithm is obtained by comparing simulations to an analytic solution of an isentropic core flow and to the two-dimensional results of an experiment.					
20 DISTRIBUTION/AVAILABILITY OF ABSTRACT <input checked="" type="checkbox"/> UNCLASSIFIED/UNLIMITED <input type="checkbox"/> SAME AS RPT <input type="checkbox"/> DTIC USERS			21 ABSTRACT SECURITY CLASSIFICATION Unclassified		
22a NAME OF RESPONSIBLE INDIVIDUAL Kurt D. Fickie			22b TELEPHONE (Include Area Code) (301) 278-6106	22c OFFICE SYMBOL SLCBR-IB-A	

CONTENTS

1. INTRODUCTION . . . . . 1

2. ALGORITHM . . . . . 2

    2.1 Governing Equations . . . . . 2

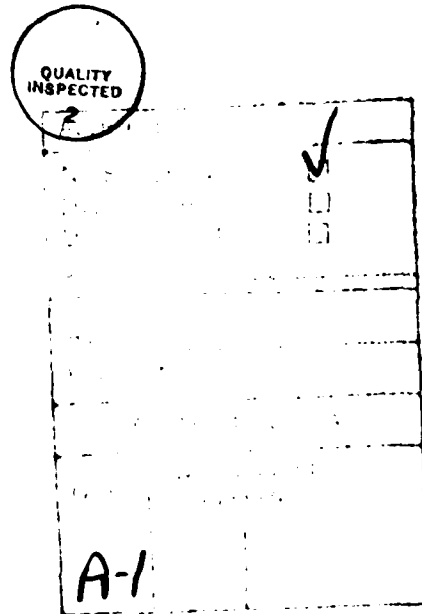
    2.2 Numerical Algorithm . . . . . 3

3. RESULTS . . . . . 15

4. SUMMARY . . . . . 18

ACKNOWLEDGMENTS . . . . . 18

REFERENCES . . . . . 19



# 1. INTRODUCTION

The flowing medium in a gun tube typically is a mixture of a compressible gas and burning solid propellant grains. Details of the flow are important for weapons development, but only bulk properties can be routinely measured, such as the trajectory of the projectile, the pressure history at a fixed station, the heating inside the gun tube, etc. Therefore, a need exists for a detailed mathematical model of interior ballistics two-phase flows, and an algorithm to solve the corresponding equations.

The three-dimensional mathematical model is developed carefully in Reference [1]. References [2] and [3] are shorter versions of Reference [1]. This two-phase model is based on instantaneous, finite volume, weighted averaging, and consists of nonlinear partial differential equations, constitutive laws for the averaged variables, and correlations for the interphase terms. The transient phenomena included in this model are: the convection of the phases driven by gas phase pressure, gas phase viscous stresses, turbulence, intergranular stresses, interphase drag, and interphase mass transfer due to burning of the solid grains; the change of energy in the gas due to convection, pressure, laminar and turbulence dissipation, conduction, and interphase heat transfer; and the change of the geometry and number of the burning grains. These phenomena occur within the volume defined by the gun tube and the base of an accelerating projectile. The motion of the projectile and the two-phase flow field are coupled via the gas pressure exerted on the projectile's base.

This model is specialized to the case of axial symmetry of the flow within the tube. Reference [1] lists all the differential equations, constitutive laws and correlations. This axial symmetric model and numerical scheme are encoded in the DELTA computer code. The purpose of this paper is to describe in some detail the numerical algorithm (Section 2), and to present some validating computer runs of the combined model and algorithm (Section 3).

Previous multi-dimensional, multi-phase work applied to interior ballistics includes that from Paul Gough Associates, Inc. [4-5], and Scientific Research Associates, Inc. [6-7]. Gough's work addresses the inviscid flow during the ballistic cycle, i.e. the average gas phase viscous stresses, heat conduction, and turbulence are excluded. Thus, the phenomenology of pressure waves inside a gun tube is modeled primarily in Gough's work. Scientific Research Associates considered the viscous flow phenomena, i.e. the development of boundary layers inside a gun tube. The work reported here resembles that of Scientific Research Associates; however, the model is somewhat different (the governing equations, choice of dependent variable, some correlations) and numerical algorithm has been modified. Differences and similarities in the models are addressed in detail in Reference [1], and in the algorithm in Section 2 of this paper.

## 2. ALGORITHM

### 2.1 Governing Equations

The governing equations are a set of nonlinear partial differential equations which are first order in time and second order in the two spatial coordinates. The rationale for the specific form of the equations is given in Reference [1]. The general form is

$$y_t = G(r, z, t, y, y_r, y_z, y_{rr}, y_{rz}, y_{zz}), \quad (2.1)$$

where the independent variables of time, radial coordinate and axial coordinate are denoted by  $t, r, z$ , respectively. The vector of dependent variables is denoted by  $y$ , and the partial derivatives of  $y$  with respect to the spatial and temporal coordinates are denoted by subscripts. The components of the vector  $y$  can be the radial, circumferential (swirl), axial components of the gas phase velocity  $(u, v, w)$ , respectively; the radial, circumferential (swirl), axial components of the solid phase velocity  $(u^*, v^*, w^*)$ , respectively; the gas phase specific entropy  $s$ ; the logarithm of gas phase pressure  $q$ ; the regression distance of the solid phase  $d^*$ ; the number of particles  $m^*$ ; the particle surface temperature  $T^*$ ; and two variables to define the turbulence in the flow field. Thus, depending on the simulation, the number of dependent variables change from a minimum of four to a maximum of thirteen. For the case of an one-phase, laminar flow simulation with swirl, the dependent vector  $y$  has five components,  $u, v, w, s$  and  $q$ . For the case of a two-phase, turbulent flow simulation with ignition and burning of the solid phase, the dependent vector  $y$  has nine components,  $u, w, u^*, w^*, s, q, d^*, m^*, T^*$ . This assumes the absence of swirl and an algebraic turbulence model (i.e. the turbulence properties are described only by algebraic relations). The components of the vector  $G$  are nonlinear functions which can depend on the variables  $r, z, t, y, y_r, y_z, y_{rr}, y_{rz}, y_{zz}$ .

The spatial domain is a confined volume within a tube bounded in length by a stationary wall (the gun breech) and the base of an accelerating projectile. The radius of the tube can depend on the axial position from the breech which is denoted by  $z_B$ . The radial coordinate varies from the axis of symmetry to the tube wall. The radial positions of the axis and wall are denoted by  $r_A$  and  $r_w(z)$ , respectively. The axial coordinate varies from the breech to the base of the projectile. The axial position of the breech and projectile base may have a radial dependence which is denoted by  $z_B(r)$  and  $z_p(r)$ , respectively.

The projectile is assumed to move as a rigid body. The unsteady projectile motion is governed by the following equations:

$$w_p = \frac{dz_p(r_A, t)}{dt}, \quad (2.2)$$

$$\frac{dw_p(t)}{dt} = \frac{1}{m_{AUG}} \left\{ 2\pi \int_{r_A}^{r_w(z_p)} p(r, z_p, t) r dr - F_A - F_D - F_B \right\}, \quad (2.3)$$

$$m_{AUG} = m_p + I_m \left[ \frac{\theta_R}{r_w(z_p)} \right]^2, \quad (2.4)$$

$$v_p(r, t) = w_p(t) \theta_R \frac{r - r_A}{r_w - r_A}, \quad (2.5)$$

where  $w_p$ ,  $v_p$ ,  $m_p$  denote the axial velocity, circumferential velocity and mass of the projectile, respectively. The forces that retard the motion of the projectile are those due to air resistance, friction between the projectile and tube wall, and gas leakage around the projectile, and are denoted by  $F_A$ ,  $F_D$ , and  $F_B$ , respectively. These retarding forces are assumed to be known functions. If the tube is rifled, an additional phenomenon is present which causes the projectile to rotate, and its mass to be effectively increased via equation (2.4). In this case the angle of rifling  $\theta_R$  is nonzero, and the moment of inertia of the projectile  $I_m$  must be given. Because the pressure  $p$  is determined from the solution of governing equations of the flow field, which depends on the value of  $w_p$ , equations (2.1) - (2.5) represent a coupled system with a moving boundary.

## 2.2 Numerical Algorithm

We want to compute by finite difference approximations the transient values of the variables which describe the fluid dynamics of the flow in the region confined by the inner tube wall, breech, and moving projectile. One way to calculate in this expanding computational region is by an "accordion" type grid in the axial direction, i.e. the first and last axial grid points are attached to the breech and projectile, respectively, and the mesh expands as the projectile accelerates down the tube. Thus, the physical grid moves in accordance with the projectile motion. With regard to the spatial finite difference approximation, the goal is to obtain an accurate approximation to the actual physical happening. It can be shown that the finite difference approximations to the physical variables in the physical mesh are the same whether one directly differences on the physical grid, or one differences on a transformed grid and then transforms back to the physical grid. Higher accuracy in a transformed space is not meaningful if it is lost in the transformation back to the physical space. Furthermore, our physical grids will be orthogonal or nearly orthogonal. Thus, we choose to compute finite difference approximations to spatial derivatives on the physical grid. An additional advantage of our method is that the governing equations need not be transformed, and thus are simpler to understand and change in the computer code.

The finite differencing of the time derivatives can be of two generic types: implicit or explicit (See Reference [8]). The principal advantage of an implicit scheme is its superior stability properties compared to an explicit scheme. For convection-diffusion type problems like those given by equation (2.1), an explicit finite difference method has two stability conditions, the Courant-Friedrichs-Lewy condition and the viscous stability limits. In one dimension, these conditions are:

$$\Delta t = \text{CFL} \frac{\Delta x}{c + w} , \quad (2.6)$$

$$\Delta t = \text{VSL} \frac{\rho}{2\mu} (\Delta x)^2 ,$$

where  $\Delta x$  is the spatial mesh increment,  $c$  is the sound speed,  $w$  is the gas velocity,  $\mu$  is the viscosity and  $\rho$  is the density. The constants CFL and VSL are less than or equal to one. For simulations which involve boundary layers, small grid sizes are necessary. Thus, for this type of simulation, the time step (the size of  $\Delta t$ ) must be proportional to the square of the smallest grid increment for an explicit scheme. On the other hand, most implicit schemes have no corresponding stability conditions, and significantly larger time steps based on accuracy considerations rather than stability can be used. The basic disadvantage of implicit algorithms is that they tend to be more complicated than explicit schemes, and thus more difficult to understand and implement. In particular, applying a standard implicit scheme to system of equations (2.1), we obtain a nonlinear system of algebraic equations in the variables at the new time level. This system can be quite large and complex because it possesses an equation for each dependent variable and for each grid point in the two-dimensional computational mesh. These equations are coupled via the spatial derivatives. Iterative methods are the most common solution procedure, but they can be quite complex and time-consuming for such a general system. To mitigate these undesirable characteristics, we apply a method developed in References [9-11]. A salient feature of this method is the temporal linearization of the nonlinear terms to within the local truncation error of the finite difference approximation of the time derivative. The resulting system can then be represented in a matrix equation,

$$\mathbf{A} \mathbf{y}^n = \mathbf{b} \quad (2.7)$$

where  $\mathbf{y}^n$  is the vector of unknown dependent variables at the new time level, and  $\mathbf{A}$  and  $\mathbf{b}$  are the matrix and vector of values at the known time level, respectively. Furthermore, the matrix  $\mathbf{A}$  can be structured if we decompose the time-differenced equation of (2.1) into two systems of equations, each of which involves the spatial derivatives of the unknown variable in only one coordinate direction. This decomposition or splitting is done so that the error incurred is of the order of the local temporal truncation error, and so that the decomposed or split equations still form a consistent approximation to equation (2.1). When centered differences are used to approximate the spatial derivatives, tridiagonal matrices are obtained. Because we are dealing with a system of equations, the matrices are block tridiagonal where the size of the blocks is

equal to the number of dependent variables. This method of splitting the implicitly differenced equations is called an Alternating Direction Implicit (ADI) scheme (see Reference [8]). Because we have also linearized the equations, we shall refer to this method as a linearized ADI scheme.

This general linearized ADI scheme is applied to the instantaneous, finite-volume, weighted, averaged equations of interior ballistics with several unique features: The algorithm is derived for a moving coordinate system, and has no mass source due to the motion of the grid. The elements of the matrices derived by the linearization process are obtained directly by numerical differentiation which bypasses the tedious and error prone task of analytically deriving each element, and the subsequent coding of these complex expressions. The spatial differencing is performed directly on nonuniform distributed grids.

### 2.2.1 Algorithm for Non-Boundary, Non-Center-Line Points

We derive the numerical scheme for the system of equations (2.1) on a moving coordinate system; i.e., the coordinates of the spatial grid system varies in time. We let the superscripts  $n$  denote the new time level and  $c$  the current time level. The change in the  $j^{\text{th}}$  coordinate position of a spatial coordinate  $x$  from level  $c$  to  $n$  is denoted by

$$\Delta x_j = x_j^n - x_j^c = \left[ \frac{\partial x}{\partial t} \right]_{t=t^c} (t^n - t^c) = O(\Delta t), \quad t^c < t^* < t^n, \quad (2.8)$$

where  $\Delta t = t^n - t^c$ . A Taylor expansion of  $y^n = y(r^n, z^n, t^n)$  about the current values at  $(r^c, z^c, t^c)$  is

$$\begin{aligned} y^n = & y^c + \frac{\partial y^c}{\partial t} \Delta t + \frac{\partial y^c}{\partial z} \Delta z + \frac{\partial y^c}{\partial r} \Delta r \\ & + \frac{1}{2} \left[ \frac{\partial^2 y^c}{\partial t^2} \Delta t^2 + 2 \Delta t \Delta z \frac{\partial^2 y^c}{\partial t \partial z} + 2 \Delta t \Delta r \frac{\partial^2 y^c}{\partial t \partial r} \right. \\ & \left. + 2 \Delta r \Delta z \frac{\partial^2 y^c}{\partial r \partial z} + \frac{\partial^2 y^c}{\partial r^2} \Delta r^2 + \frac{\partial^2 y^c}{\partial z^2} \Delta z^2 \right] + O(\Delta t^3). \end{aligned} \quad (2.9)$$

By adding  $(1 - \beta)$  times (2.9) and  $\beta$  times a similar expansion to (2.9) of  $y^c$  expanded about  $y^n$ , and noting that  $y^n - y^c = O(\Delta t)$ ,  $z^n - z^c = O(\Delta t)$ , and  $r^n - r^c = O(\Delta t)$ , we obtain

$$\begin{aligned}
& \mathbf{y}^n - \beta \Delta t \mathbf{G}^n - \beta \Delta r \left[ \frac{\partial \mathbf{y}}{\partial r} \right]^n - \beta \Delta z \left[ \frac{\partial \mathbf{y}}{\partial z} \right]^n \\
& = \mathbf{y}^c + (1-\beta) \Delta t \mathbf{G}^c + (1-\beta) \Delta r \left[ \frac{\partial \mathbf{y}}{\partial r} \right]^c + (1-\beta) \Delta z \left[ \frac{\partial \mathbf{y}}{\partial z} \right]^c \\
& \quad + (\beta - \frac{1}{2}) O(\Delta t^2) + E_T(\Delta t^3), \quad \frac{1}{2} \leq \beta \leq 1.0,
\end{aligned} \tag{2.10}$$

where  $E_T(\Delta t^3)$  denotes the neglected truncation error of  $O(\Delta t^3)$ . For a stationary grid  $\Delta r = \Delta z = 0$ , we obtain the standard Crank-Nicolson scheme for integration parameter  $\beta = \frac{1}{2}$  and the standard fully implicit scheme for  $\beta = 1.0$ . Equation (2.10) is a nonlinear system of equations in  $\mathbf{y}^n$  because  $\mathbf{G}^n$  is a nonlinear function. To make (2.10) a system of linear equations, we linearize  $\mathbf{G}^n$  via a Taylor expansion about the current level, i.e.

$$\begin{aligned}
\mathbf{G}^n & = \mathbf{G}^c + \left[ \frac{d\mathbf{G}}{dt} \right]^c \Delta t + E_{Ll}(\Delta t^2) \\
& = \mathbf{G}^c + \left[ \frac{\partial \mathbf{G}}{\partial t} \right]^c \Delta t + \left[ \frac{\partial \mathbf{G}}{\partial r} \right]^c \Delta r + \left[ \frac{\partial \mathbf{G}}{\partial z} \right]^c \Delta z \\
& \quad + D^c \Delta \mathbf{y} + DR^c \Delta \mathbf{y}_r + DZ^c \Delta \mathbf{y}_z \\
& \quad + DRR^c \Delta \mathbf{y}_{rr} + DRZ^c \Delta \mathbf{y}_{rz} + DZZ^c \Delta \mathbf{y}_{zz} \\
& \quad + E_{Ll}(\Delta t^2),
\end{aligned} \tag{2.11}$$

where  $E_{Ll}(\Delta t^2)$  denotes the neglected linearization error of  $O(\Delta t^2)$ . The Jacobian type matrices are denoted by  $D, DR, DZ, DRR, DRZ, DZZ$ , are evaluated at the current time level, and are defined as

$$D_{ij}^c \equiv \left[ \frac{\partial \mathbf{G}_i}{\partial \mathbf{y}_j} \right]^c, \quad DR_{ij}^c \equiv \left[ \frac{\partial \mathbf{G}_i}{\partial \mathbf{y}_{r_j}} \right]^c, \quad \dots, \quad DZZ_{ij}^c \equiv \left[ \frac{\partial \mathbf{G}_i}{\partial \mathbf{y}_{z_j}} \right]^c. \tag{2.12}$$

Upon substituting (2.11) into (2.10), we obtain the following linear system of equations in  $\mathbf{y}^n$  after algebraic manipulation:

$$\begin{aligned}
& \mathbf{y}^n - \beta \left\{ \Delta r \left[ \left( \frac{\partial \mathbf{y}}{\partial r} \right)^n + \Delta z \left( \frac{\partial \mathbf{y}}{\partial z} \right)^n + \Delta t \left[ D^c \mathbf{y}^n + DR^c \left( \frac{\partial \mathbf{y}}{\partial r} \right)^n + DZ^c \left( \frac{\partial \mathbf{y}}{\partial z} \right)^n \right. \right. \right. \\
& \quad \left. \left. \left. + DRR^c \left( \frac{\partial^2 \mathbf{y}}{\partial r^2} \right)^n + DRZ^c \left( \frac{\partial^2 \mathbf{y}}{\partial r \partial z} \right)^n + DZZ^c \left( \frac{\partial^2 \mathbf{y}}{\partial z^2} \right)^n \right] \right\} \quad (2.13) \\
& = \mathbf{y}^c - \beta \left\{ \Delta r \left[ \left( \frac{\partial \mathbf{y}}{\partial r} \right)^c + \Delta z \left( \frac{\partial \mathbf{y}}{\partial z} \right)^c + \Delta t \left[ D^c \mathbf{y}^c + DR^c \left( \frac{\partial \mathbf{y}}{\partial r} \right)^c + DZ^c \left( \frac{\partial \mathbf{y}}{\partial z} \right)^c \right. \right. \right. \\
& \quad \left. \left. \left. + DRR^c \left( \frac{\partial^2 \mathbf{y}}{\partial r^2} \right)^c + DRZ^c \left( \frac{\partial^2 \mathbf{y}}{\partial r \partial z} \right)^c + DZZ^c \left( \frac{\partial^2 \mathbf{y}}{\partial z^2} \right)^c \right] \right\} \\
& \quad + \Delta r \left[ \left( \frac{\partial \mathbf{y}}{\partial r} \right)^c + \Delta z \left( \frac{\partial \mathbf{y}}{\partial z} \right)^c + \Delta t \mathbf{G}^c + \beta \Delta t \left[ \Delta t \left( \frac{\partial \mathbf{G}}{\partial t} \right)^c + \Delta r \left( \frac{\partial \mathbf{G}}{\partial r} \right)^c \right. \right. \\
& \quad \left. \left. + \Delta z \left( \frac{\partial \mathbf{G}}{\partial z} \right)^c \right] + (\beta - \frac{1}{2}) O(\Delta t^2) + E_T(\Delta t^3) + E_{Ll}(\Delta t^3).
\end{aligned}$$

The neglected linearization error  $E_{Ll}$  is now  $O(\Delta t^3)$  because  $\mathbf{G}^n$  was multiplied by  $\Delta t$  in (2.10). Thus, the linearization process does not alter the order of the temporal error.

The values  $\mathbf{y}^c, r^c, z^c, t^c, r^n, z^n, t^n$  are all known before the start of the integration routine to determine the values of  $\mathbf{y}^n$ . Thus, the right hand side of (2.13) is a known vector. The left hand side of (2.13) can be written as a matrix with known values times a vector of unknowns,  $\mathbf{y}^n$ . Thus, (2.13) has the form of (2.7). The matrix  $\mathbf{A}$  interconnects values of  $\mathbf{y}^n$  at a grid point to all the values of its spatial neighbors via the first and second spatial partial derivatives at level  $n$ . If the term  $\left[ \left( \frac{\partial^2 \mathbf{y}}{\partial r \partial z} \right)^n \right]$  were absent from the left hand side of (2.13), we could decompose (2.13) into two matrix equations which are highly structured and easily solvable while still retaining only two time levels of the dependent variable vector, i.e.  $\mathbf{y}^n$  and  $\mathbf{y}^c$ . To this end, we linearize the mixed derivative at the  $n$  level about the current level and retain only the leading term:

$$\left[ \frac{\partial^2 \mathbf{y}}{\partial r \partial z} \right]^n = \left[ \frac{\partial^2 \mathbf{y}}{\partial r \partial z} \right]^c + E_{LA}(\Delta t). \quad (2.14)$$

Substituting (2.14) into (2.13), we obtain after some algebraic manipulations

$$\begin{aligned} \left[ \mathbf{I} - \beta(D_r^n + D_z^n) \right] \mathbf{y}^n &= \left[ \mathbf{I} - \beta(D_r^c + D_z^c) \right] \mathbf{y}^c + L \mathbf{y}^c \\ &= (\beta - \frac{1}{2})O(\Delta t^2) + E_T(\Delta t^3) + E_{L'}(\Delta t^3) + E_{LA}(\Delta t^2), \end{aligned} \quad (2.15a)$$

where the operators are defined as follows:

$$D_r^k \equiv \Delta r \left[ \frac{\partial}{\partial r} \right]^k + \Delta t \left[ D^c + DR^c \left[ \frac{\partial}{\partial r} \right]^k + DRR^c \left[ \frac{\partial^2}{\partial r^2} \right]^k \right], \quad (2.15b)$$

$$D_z^k \equiv \Delta z \left[ \frac{\partial}{\partial z} \right]^k + \Delta t \left[ DZ^c \left[ \frac{\partial}{\partial z} \right]^k + DZZ^c \left[ \frac{\partial^2}{\partial z^2} \right]^k \right], \quad (2.15c)$$

$$\begin{aligned} L \mathbf{y}^c &\equiv \Delta r \left[ \frac{\partial \mathbf{y}}{\partial r} \right]^c + \Delta z \left[ \frac{\partial \mathbf{y}}{\partial z} \right]^c + \Delta t \mathbf{G}^c \\ &+ \beta \Delta t \left[ \Delta t \left[ \frac{\partial \mathbf{G}}{\partial t} \right]^c + \Delta r \left[ \frac{\partial \mathbf{G}}{\partial r} \right]^c + \Delta z \left[ \frac{\partial \mathbf{G}}{\partial z} \right]^c \right]. \end{aligned} \quad (2.15d)$$

The symbol  $\mathbf{I}$  represents the identity matrix, and the superscript  $k$  can be either  $n$  or  $c$ . The "lagging" of the mixed derivative (2.14) increased the error of the approximation to  $O(\Delta t^2)$  for any value of the integration parameter  $\beta$ , but we gain a structured matrix.

We can decompose (2.15a) along coordinate directions in the following manner:

$$\left[ \mathbf{I} - \beta D_r^n \right] \mathbf{y}^I = \left[ \mathbf{I} - \beta D_r^c \right] \mathbf{y}^c + L \mathbf{y}^c, \quad (2.16)$$

$$\left[ \mathbf{I} - \beta D_z^n \right] \mathbf{y}^F = \left[ \mathbf{I} - \beta D_z^c \right] \mathbf{y}^c + (\mathbf{y}^I - \mathbf{y}^c). \quad (2.17)$$

Equation (2.16) constitutes the radial sweep of this Alternating Direction Implicit method because it involves only spatial derivatives in the radial direction at the new time level. One solves this equation for each fixed axial index and for radial indices varying from the axis of

symmetry to the gun tube wall. When three point centered spatial finite differences are used to approximate the spatial derivatives in the radial direction, the matrix  $\mathbf{I} - \beta D_r^n$  is a block tridiagonal matrix. The size of each block is equal to the number of dependent variables. The number of block rows is equal to the number of grid points from the axis of symmetry to the gun tube wall, denoted by  $JRMX$ . The block rows from the second grid points to one away from the wall, namely  $JRMX - 1$  is determined by (2.16). The entries of the first and last block rows are determined from the conditions imposed at the axis of symmetry and wall, respectively. The right hand side of (2.16) is a known vector because it is evaluated at the current time-step. The solution of this equations is the intermediate values of the dependent variables  $y^I$ .

Equation (2.17) constitutes the axial sweep of this two sweep scheme because it involves only the spatial derivatives in the axial direction at the new time level. One solves this equation for each fixed radial index and for axial indices varying from the breech to the base of the projectile. The matrix  $\mathbf{I} - \beta D_z^n$  is a block tridiagonal matrix when three point centered spatial finite differences are used to approximate the partial derivatives in the axial direction. The size of the blocks are the same as in the radial sweep, and the number of block rows is equal to the number grids points placed from the breech to the projectile base, denoted by  $JZMX$ . Equation (2.17) is used to determine the entries in the block rows from the second point (one after the breech) to  $JZMX - 1$  (one before the projectile base). The entries in the first and last block rows are determined from the boundary conditions imposed at the breech and projectile base, respectively. Because the intermediate value  $y^I$  is known, the right hand side of (2.17) is known. The solution of (2.17) is the value of the dependent variables at the new time level, denoted by  $y^F$ . The values of the solution vector  $y^F$  of (2.17) and those of the solution vector  $y^n$  of (2.15) differ by the time error introduced by the splitting (2.16)-(2.17). To determine the order of this error, we substitute (2.17) into (2.16) and obtain

$$(\mathbf{I} - \beta D_r) \left[ (\mathbf{I} - \beta D_z) y^F - (\mathbf{I} - \beta D_z) y^c + y^c \right] = [\mathbf{I} - \beta D_r] y^c + L y^c \quad (2.18)$$

which simplifies to

$$(\mathbf{I} - \beta D_r - \beta D_z) y^F = (\mathbf{I} - \beta D_r - \beta D_z) y^c + L y^c - \beta^2 D_r D_z (y^F - y^c). \quad (2.19)$$

Subtracting (2.15a) from (2.19), have

$$(\mathbf{I} - \beta D_r - \beta D_z) (y^F - y^n) = -\beta^2 D_r D_z (y^F - y^n + y^n - y^c) \quad (2.20)$$

or

$$(\mathbf{I} - \beta D_r - \beta D_z + \beta^2 D_r D_z) (y^F - y^n) = -\beta^2 D_r D_z (y^n - y^c). \quad (2.21)$$

We note that the coefficient of  $y^F - y^n$  is  $O(1)$ ,  $D_r$  and  $D_z$  are each  $O(\Delta t)$  and  $(y^n - y^c)$  is

at least  $O(\Delta t)$ . Thus,

$$\mathbf{y}^F = \mathbf{y}^n + E_S(\Delta t^3), \quad (2.22)$$

that is,  $\mathbf{y}^F$  is equal to  $\mathbf{y}^n$  to within the local truncation error of the scheme.

Equations (2.16), (2.17) with the definitions (2.15b)-(2.15d) represent the time differenced, linearized, ADI scheme. We now turned to the finite difference approximation of the spatial derivatives. The standard centered finite difference approximations to the spatial partial derivatives in the coordinate direction  $x$  at the  $i^{\text{th}}$  grid point are

$$\left[ \frac{\partial \mathbf{y}}{\partial x} \right]_i \approx \frac{h_i (y_i - y_{i-1})}{h_{i-1}(h_i + h_{i+1})} + \frac{h_{i-1}(y_{i+1} - y_i)}{h_i (h_i + h_{i+1})}, \quad (2.23)$$

$$\left[ \frac{\partial^2 \mathbf{y}}{\partial x^2} \right]_i \approx \frac{2(y_{i-1} - y_i)}{h_{i-1}(h_i + h_{i-1})} + \frac{2(y_{i+1} - y_i)}{h_i (h_i + h_{i-1})}, \quad (2.24)$$

where  $h_i \equiv x_{i+1} - x_i$ . However, instead of (2.23) we use

$$\frac{\partial y_i}{\partial x} = \frac{(y_{i+1} - y_{i-1})}{(h_i + h_{i-1})}. \quad (2.25)$$

(See Reference 12). For equally spaced meshes (2.23) and (2.25) are identical. For a nonuniform spaced grid, the difference between them can be expressed as

$$\frac{1}{2}(h_{i-1} - h_i) \frac{\partial^2 \mathbf{y}}{\partial x^2}. \quad (2.26)$$

The nonuniform grids that are used in our application have the property that  $h_{i-1} \geq h_i$  so that (2.26) acts as a stabilizing viscous term to the spatial differencing.

To complete the description of the interior point algorithm we discuss the determination of the Jacobian type matrices  $D$ ,  $DR$ ,  $DZ$ ,  $DRR$ ,  $DZZ$  defined by (2.12). The obvious way to evaluate the elements of these matrices is to manually take the partial derivatives and code each element. This double procedure is very error prone because the right hand sides of the equations are extremely complex. If there are  $NEQ$  variables, then each element of the vector  $G$  is a function of  $6*NEQ + 3$  arguments, in general. Furthermore, for two-phase simulations, the correlations are not fixed, but can vary substantially from simulation to simulation. In these cases new elements of the matrices would have to be determined and encoded. To avoid this, one can lag the contribution of these correlations by one time step. This is not totally desirable because one increases the local truncation error (see the discussion near (2.14)) which can be large when the correlations add significantly to the flow dynamics in a given time step, e.g.,

burning of the grains. An alternative to this whole procedure is to determine these matrices numerically. Consider the determination of  $D_{ij} \equiv \frac{\partial G_i}{\partial y_j}$  which can be approximated by

$$D_{ij} \approx \left[ G_i(r, z, t, y_1, \dots, y_j + \delta, \dots, y_{NEQ}, y_r, \dots, y_z) - G_i(r, z, t, y_1, \dots, y_j - \delta, \dots, y_{NEQ}, y_r, \dots, y_z) \right] / (2\delta), \quad (2.27)$$

where  $\delta$  is the pre-determined increment. Once these increments are obtained, the elements of the matrices can be computed trivially by repeated calls to a subroutine which computes the right hand sides of the equations. A characteristic of the  $G$ 's is that the terms  $y_r$  and  $y_z$  appear at most quadratically, and the terms  $y_r$  and  $y_z$  appear at most linearly. Thus, by using centered differences the matrices  $DR$  and  $DZ$  can be obtained exactly for any value of the increment. Likewise, using one-side differences the matrices  $DRR$  and  $DZZ$  can be determined exactly. In these cases, a large value of the increment can be used to avoid any round off errors. On the other hand the vector  $G$  is a non-algebraic, nonlinear function of the vector  $y$ . In this case one cannot obtain an exact value of the elements of  $D$  for any value of the increment. We have developed a strategy to compute an increment value based on the current error estimates of  $G_i$  and  $y_j$ , that is, to determine  $D_{ij}$  a  $\delta_{ij}$  is used. The drawback of this approach is the computing time necessary to evaluate the right hand sides as often as required.

Finally, we address the problem of artificial mass sources induced solely by the motion of a grid system. The problem was illustrated and resolved in Reference 13. There exists a standard procedure to determine if mass sources occur in a numerical scheme when the grids are moved. First one assumes a constant flow field at the current level, secondly one applies the method to compute the new time level of values on a displaced grid, and finally one determines if these new values differ from the constant values. Following this procedure, we assume that the flow field variables are constants which satisfy the partial differential equations, and assume that  $\Delta r \neq 0$  and  $\Delta z \neq 0$ . Consequently, all the spatial derivatives at the current time level are zero and (2.13) reduces to

$$\begin{aligned} y^n - \beta \left\{ \Delta r y_r^n + \Delta z y_z^n \right. \\ \left. + \Delta t \left[ D y^n + DR y_r^n + DZ y_z^n + DRR y_r^n + DRZ y_r^n + DZZ y_z^n \right] \right\} \\ = y^c - \beta \Delta t D y^c. \end{aligned} \quad (2.28)$$

Using the fact that the spatial derivatives at the current level are zero, we add zero to (2.28) in a convenient form to obtain

$$\mathbf{A}(\mathbf{y}^n - \mathbf{y}^c) = 0, \quad (2.29)$$

where  $\mathbf{A}$  is a matrix. If  $\mathbf{A}$  is nonsingular, then the solution of (2.29) is  $\mathbf{y}^n = \mathbf{y}^c$ . Thus, no mass sources exist. The lack of mass sources is due to the form of the equations, i.e.  $\mathbf{y}_i = \mathbf{G}$ , and the algorithm. For a simpler set of equations than the one we are solving, and for a set in a conservation form which are transformed to a stationary uniform computational grid, a "Geometric Conservation Law" is needed to prevent mass sources. (See Reference 13). Our method automatically avoids this other partial differential equation, and the need to obtain its solution at every time step.

### 2.2.2 Algorithm for Points at the Center-Line and at the Solid Surfaces

The method to obtain the new time level of the flow variables along the center-line is different. To maintain the axial symmetry of the flow, the physical conditions on the flow are the radial and circumferential velocity components for both the gas and particle phases must be zero, and the first partial derivatives with respect to the radial direction at the axis of symmetry of the remaining variables must be zero.

The contribution from the points on the axis of symmetry can be done in at least two ways. The first and simplest is to directly apply the symmetry conditions. For a radial sweep, the elements of the first block row of the matrix  $\mathbf{A}$  and known vector  $\mathbf{b}$  are the finite difference approximations of these conditions. The axial sweep along the center-line is performed after the axial sweeps along interior axial indices. The final values at the center-line are obtained using the symmetry conditions, and the final axial sweep values of the non-center-line points. The second way is more complex. Because the center-line is part of the flow field (physically a non-boundary), the governing partial differential equations are valid on the axis of symmetry. One may rewrite these equations with the symmetry conditions imposed in the equations themselves, and with the correct limit conditions as the radial coordinate goes to zero. Then, solve these new equations by exactly the same method as described for non-boundary points. Although both are coded, the simpler first option is utilized.

The boundary conditions at the solid surfaces such as the breech, tube wall and projectile base can vary substantially with the particular simulation. This makes a general discussion of boundary conditions difficult. However, we will discuss some implementations of common types of boundary conditions. The simple functional form boundary condition  $y = \text{constant}$ , and the simple derivative boundary condition  $\frac{\partial y}{\partial x} = \text{constant}$  are the most trivial kinds. Their finite difference approximations are straightforward, if  $y$  is a variable computed directly by a governing partial differential equation, i.e., one of the variables in (2.1). However, if one has a

nonlinear boundary condition of the form  $f(y)^n = 0$  or  $f\left(\frac{\partial y}{\partial x}\right)^n = 0$ , then one must linearize function  $f$  in time in the same manner as is any component of the nonlinear vector function  $G$  in (2.1) and (2.11).

Sometimes a nonlinear boundary condition can be reformulated as a linear one. Consider the adiabatic condition  $\left(\frac{\partial T}{\partial \mathbf{n}}\right)^n = 0$  where  $T$  is the temperature and  $\mathbf{n}$  is the outward normal. In our method the entropy  $s$  and pressure function  $q$  are computed directly from the governing partial differential equations. Thus  $T$  is a nonlinear function,  $T = T(s, q)$ . We ordinarily would expand  $\left(\frac{\partial T}{\partial \mathbf{n}}\right)^n$  in a Taylor series in time to obtain a linear function in  $s^n$  and  $q^n$ . However, for a Noble-Abel equation of state, we have a simplification. We use the chain rule to obtain

$$\left( \frac{\partial T}{\partial s} \frac{\partial s}{\partial \mathbf{n}} + \frac{\partial T}{\partial q} \frac{\partial q}{\partial \mathbf{n}} \right)^n = 0. \quad (2.30)$$

Since  $\frac{\partial T}{\partial s} \neq 0$ , then (2.30) can be written as

$$\left( \frac{\partial s}{\partial \mathbf{n}} + \frac{\frac{\partial T}{\partial q}}{\frac{\partial T}{\partial s}} \frac{\partial q}{\partial \mathbf{n}} \right)^n = 0. \quad (2.31)$$

By noting that the ratio of partial derivatives of temperature is a constant, (2.31) is a linear function in  $s^n$  and  $q^n$ . Thus, (2.31) can be finite differenced and incorporated directly into the matrices of the linearized ADI method.

### 2.2.3 The Order of the Sweeps

The order of the sweeps is mainly a bookkeeping problem, and should not have a large effect on the solution. We have used the following procedure. First, radial sweeps from the center-line to the tube wall are performed along constant axial indices to obtain intermediate values of the variables  $y$  using (2.16). The axial index varies from the one after the breech to the one before the projectile base. Second, axial sweeps from the breech to the projectile base are performed along constant radial indices to obtain values of the variables  $y$  at the new time level using (2.17). The radial index varies from the one after the axis of symmetry to the one before the gun tube wall. Third, the symmetry conditions are applied to determine the new time level values at all points on the axis of symmetry by using the results of the axial sweep

are determined by imposing the wall boundary condition using, if necessary, the results of the axial sweep (step two).

We note that the radial sweeps along the breech and projectile are avoided. The justification is that in many applications the boundary conditions at the breech and projectile do not involve radial derivatives. Consequently, the linearized version of these conditions can be expressed without the need for the determination of the intermediate values of the variables. Recall that the matrix  $\mathbf{D}$  (equation (2.12)) was included in the radial sweep. (See equations (2.15b) & (2.16)). However, it could have been incorporated into the axial sweep formula. (See equations (2.15c) & (2.17)). If no radial derivatives exist for the boundary conditions, we avoid the radial sweep and incorporate the  $\mathbf{D}$  matrix in the axial sweep formulation. An example of this type of boundary condition is the gas continuity equation used to determine the transformed pressure  $q$  at the breech for a one-phase, viscous simulation. Imposing the no-slip conditions  $u = v = w = 0$  in the continuity equation evaluated at the breech, all radial derivatives vanish, and the above method is applied directly during the axial sweep where one-sided finite differences are used to approximate the spatial derivatives at the breech. If one uses the normal velocity equation for the determination of  $q$  at the projectile base, for example, some radial derivatives remain in the viscous terms. Only by lagging them could one use the above approach.

### 3. RESULTS

The results of two simulations using the DELTA code are presented in this section. These particular calculations are selected because they can be compared to independently determined answers, and thus, give some verification of the code's accuracy and capabilities. Both cases involve a one-phase gas expansion in a constant cross-section tube closed at one end by a stationary surface called the breech, and at the other end by a movable piston called the projectile. The breech and projectile base are assumed to be flat surfaces. The initial states of the gas are uniform and quiescent, but the gas pressures are great enough to accelerate the projectile through the tube. The controlling mechanisms of the expansion flows are the same, namely the propagation of the rarefaction wave, generated by the projectile displacement, and its reflection from the breech, then the projectile, and so forth. However, the gas pressure levels differ greatly between the simulations, and the subsequent flows are in different regimes.

TABLE 1. Geometry and Gas Properties for the 150-mm Gun and Bicen-Whitelaw Experiments

150-mm Gun	Description	Bicen-Whitelaw
150.0	Bore Diameter ( <i>mm</i> )	76.7
1.698	Initial Projectile Displacement ( <i>m</i> )	0.1773
6.0	Maximum Travel of Projectile ( <i>m</i> )	0.3
50.0	Projectile Mass ( <i>kg</i> )	2.54
0.001	Covolume ( <i>m</i> <sup>3</sup> / <i>kg</i> )	0.0
1.22	Ratio of specific heats, $\gamma$	1.4
621.09	Initial Pressure ( <i>MPa</i> )	0.28
2666.8	Initial Temperature ( <i>K</i> )	293.0

The first simulation corresponds to the gas expansion within a 150-mm tube away from the effects of the tube wall (core-flow) under ballistic conditions. The specifications for this case are given by the first column of Table 1. The analytic solution of the one-dimensional, inviscid gas equations governing the flow within this 150-mm tube at certain positions from the breech and for specified times was obtained by Love and Pidduck. (See Reference [14].) Their solution is valid under the assumptions of isentropic expansion of each element of gas, of constant covolume, of an even integer value of the ratio  $(\gamma + 1)/(\gamma - 1)$ , where  $\gamma$  is the ratio of specific heats, and the frictionless motion of the projectile. The solution is in terms of truncated power

series, and becomes more complicated as the number of rarefaction wave reflections increase. For the one-dimensional DELTA calculation, the computational mesh (covering the enclosed cavity behind the projectile) consisted of four equidistant mesh lines parallel to the axis of symmetry and 89 uniformly spaced grid lines orthogonal to the axis of symmetry. To maintain a one-dimensional simulation for comparison to the Love Pidduck results, the following conditions

$$u = \frac{\partial w}{\partial r} = \frac{\partial s}{\partial r} = \frac{\partial q}{\partial r} = 0$$

are imposed along both the tube wall and axis of symmetry. The boundary conditions at the breech and projectile are no-slip velocity and adiabatic walls. Love and Pidduck developed their solution with the assumption of an inviscid isentropic flow which allowed them to use a special form of the Noble-Abel equation of state, namely

$$P \left( \frac{1}{\rho} - \eta \right)^\gamma = P_0 \left( \frac{1}{\rho_0} - \eta \right)^\gamma = \text{constant},$$

where subscript zero indicate their initial values. However, in the DELTA simulation viscous effects are included and the general form of the Noble-Abel equation of state. However, the special form of the equation of state used by Love and Pidduck is maintained to within less than two percent in the DELTA simulations. Thus, the non-isentropic and viscid effects included in the general framework of DELTA are minor for this one-dimensional flow, and the comparison of the analytic solution and numerical results is reasonable.

The comparison of the pressure histories at the projectile base is given in Figure 1. The change in slope in the pressure curve is due to the first reflection of the rarefaction wave at the projectile base. The magnitude of the slope discontinuity of the pressure curve decreases with time due to the equilibration of the pressures during the gas expansion. Another slope change exists theoretically at 7.137ms, although it cannot be detected even in the graph of the analytical results. Figure 2 is similar to Figure 1 except that the pressures at the breech are compared. The effect of the first arrival of the wave at the breech is more obvious in both solutions.

Figures 3 and 4 show comparisons of the histories of the projectile velocity and projectile displacement from the breech, respectively. The large values of the tangent to the curve in Figure 3 indicate the extreme acceleration the projectile experiences. The agreement of the results show that the numerical solution of the partial differential equations governing the gas motion using the DELTA algorithm is correctly coupled to the proper solution of the projectile motion. Comparisons of the pressure profiles from the breech to the projectile at specified times are given in Figures 5 and 6. The ranges of pressure values on the ordinate are the smallest possible to provide accurate comparisons. Figure 5 shows a comparison of the pressure values at 2.898ms, that is, after the rarefaction wave has been reflected from the breech, then the

projectile base, and is approximately halfway between them. The DELTA calculation differs by 0.6% at most from the analytic solution values. The slope discontinuity is smeared out in the numerical calculation. Figure 6 shows the pressure profiles at 10.23ms which is near tube-exit time of the projectile. The maximum discrepancy between the two results is approximately 1.2%. Because the analytic solution is a truncated power series solution, it is difficult to determine which values are more accurate.

Next we compare a DELTA simulation with time-resolved measurements of the axial velocity field inside a tube behind a slowly accelerating projectile obtained by laser-Doppler anemometry. The experiment was performed at Imperial College, London under funding by European Research Office of the Army and The Ballistic Research Laboratory, and is reported in Reference [15]. This experiment is important to the development of DELTA because it provides the first transient, two-dimensional measurements of a quantity to which the results of a DELTA simulation can be compared. The schematic of the apparatus is given in Figure 7. Nitrogen is the gas, and the other characteristic of the experiment are given in the second column of Table 1.

Three important conclusions of this study are: The maximum intensity level of the turbulence was approximately four percent which implies a very low level of turbulence, the tube wall boundary layer remained laminar, and the heat transfer to the tube wall was minimal. Consequently, a laminar flow simulation with adiabatic walls should approximate this experiment. The two-dimensional computational grid had 33 uniformly distributed points in the axial direction, and 19 nonuniformly distributed points in the radial direction. The radial grid was such that, while 19 points spanned the distance from the axis of symmetry ( $r = 0$ ) to the wall ( $r = 38.35mm$ ), 12 points were distributed from  $r = 32mm$  to the wall and 5 points were distributed from  $r = 37.85mm$  to the wall. The maximum and minimum distance between the grid points were  $6.5mm$  and  $70\mu m$ , respectively. Constant values were used for the coefficients of viscosity and thermal conductivity of nitrogen, namely,  $17.07\mu(Pa\cdot s)$  and  $0.02524W/(m\cdot K)$ , respectively. Because the experimental apparatus was mounted vertically, the equation for the projectile motion (2.3) was changed to include its acceleration due to gravity. Because the total retarding force ( $F_D + F_B + F_A$  in (2.3)) experienced by the projectile was not determined by the experiment, no values of these forces could be assigned. Thus, a total retarding force profile versus axial displacement was obtained so that the axial velocity of the projectile determined by the DELTA code matched the experimental values as shown in Figure 8. Because the projectile velocity values agree, so must the projectile displacement values. Figure 9 compares the axial velocity profiles along the axis of symmetry at various times. Both the DELTA and experimental results show a linear profile from the zero value at the breech to the value of the projectile velocity for each time. The axial velocity histories at 76.7mm from the breech and at 0.5, 1.0, 2.0, and 3.0mm from the tube wall are compared in Figure 10. The values from the calculation are within the scatter of the experimental data at radial positions of 1, 2 and 3mm from the wall. However, the discrepancy between the values at the 0.5mm position increases with time. The same quantities are graphed in Figure 11 but at 153.4mm from the breech. The comparisons in Figure 11 show similar behavior to that in Figure 10, but with

the discrepancy at the  $0.5\text{mm}$  position considerably larger. After a discussion with the experimentalists, it was agreed that these most difficult measurements at  $0.5\text{mm}$  from the tube wall are likely to contain errors and should be redone. We are presently awaiting accurate measurements in the sub-millimeter range. However, the present agreement between the experimental measures and calculations are encouraging.

#### 4. SUMMARY

The numerical algorithm encoded in the DELTA computer code, and comparisons of its calculations to an analytic solution and experimental measures are described.

A numerical algorithm to solve the two-dimensional, axisymmetric, unsteady, finite volume, weighted averaged two-phase equations which govern certain flows inside a gun tube is discussed. These equations are in their most general form. In particular, when the flow regime is governed only by convection and pressure forces, this general form automatically gives the solution of the corresponding inviscid equations. When in the boundary layer regime, this general form gives without any assumptions, the solution in the boundary layer where viscous forces dominate. Moreover, this approach naturally provides all the coupling between different phenomena because only one set of equations, which govern all the phenomena, is solved. Thus, phenomena that is controlled by basically inviscid flow but exists because of viscous forces, like the additive particle laden gun tube wall boundary layer which governs heat transfer to the gun tube, can be studied for the first time without assumptions on the natures of the core flow or boundary layer, the validity of heat-transfer correlations, and/or the intra-flow coupling between various regimes.

Two examples of calculations with the DELTA code are presented. These computations are limited to one-phase expansion flows in an adiabatic tube so to allow comparisons with independently obtained data. More realistic calculations that involve ballistic environments, heat transfer to the gun tube wall, and other phenomena are presented in Reference [16].

#### ACKNOWLEDGMENTS

The development of a large computer code such as DELTA can not be accomplished in any timely fashion by one man. During its evolution several have contributed ideas and/or programming time. Thomas Mann, Aivars Celmins, Rudi Heiser, Csaba Zoltani, Christopher Roller, and Stephen Davis made contributions to the development of the DELTA code. I gratefully acknowledge their efforts. Furthermore, this code was developed under the administrative supervision of Norman Banks. Without his support, this project could not have been started and nurtured.

## REFERENCES

- [1] A.K.R. Celmins and J.A. Schmitt, "Volume Averaged Two-Phase (Gas-Solid) Interior Ballistics Equations," ARBRL-TR-2593, *USA Ballistic Research Laboratory Report*, 1984.
- [2] A.K.R. Celmins and J.A. Schmitt, "Three Dimensional Modeling of Gas-Combusting Solid Two-Phase Flows," *Proceedings of the Third Multi-Phase Flow and Heat Transfer Symposium-Workshop*, T. N. Veziroglu, ed., 18-20 April 1983, Miami Beach, Florida.
- [3] A.K.R. Celmins and J.A. Schmitt, "Modeling of Gas-Solid Phenomena in Interior Ballistics," *Proceedings of The Seventh International Symposium on Ballistics*, 19-21 April 1983, The Hague, The Netherlands.
- [4] P.S. Gough, "Two-Dimensional, Two-Phase Modelling of Multi-Increment Bagged Artillery Charges," ARBRL-CR-00503, Ballistic Research Laboratory, Aberdeen Proving Ground, MD, 1982.
- [5] P.S. Gough, "Modeling of Rigidized Gun Propelling Charges," ARBRL-CR-00518, Ballistic Research Laboratory, Aberdeen Proving Ground, MD, 1983.
- [6] H.J. Gibeling and H. McDonald, "Development of a Two-Dimensional Implicit Interior Ballistic Code," ARBRL-CR-00451, Ballistic Research Laboratory, Aberdeen Proving Ground, MD, 1981.
- [7] H.J. Gibeling and H. McDonald, "An Implicit Numerical Analysis for Two-Dimensional Turbulent Interior Ballistics Flows," ARBRL-CR-00523, Ballistic Research Laboratory, Aberdeen Proving Ground, MD, 1984.
- [8] R.D. Richtmyer and K.W. Morton, **Difference Methods for Initial-Value Problems**, 2nd ed., Wiley-Interscience(New York, 1967).
- [9] W.R. Briley and H. McDonald, "Solution of the Multi-Dimensional Compressible Navier-Stokes Equations by a Generalized Implicit Method," *J. Comp. Phy.* **24** (1977) 372-397.
- [10] R.M. Beam and R.F. Warming, "An Implicit Finite-Difference Algorithm for Hyperbolic Systems in Conservation Form," *J. Comp. Phy.* **22** (1976) 87-110.
- [11] W.R. Briley and H. McDonald, "On the Structure and Use of Linearized Block Implicit Schemes," *J. Comp. Phy.* **34** (1980) 54-73.
- [12] E. Kalnay de Rivas, "On the Use of Nonuniform Grids in Finite-Difference Equations," *J. Comp. Phy.* **10** (1972) 202-210.
- [13] P.D. Thomas and C.K. Lombard, "Geometric Conservation Law and Its Application to Flow Computations on Moving Grids," *AIAA Journal* **17** (1979) 1030-1036.
- [14] E.H. Love and F.B. Pidduck, "Lagrange's Ballistic Problem," *Phil. Trans. Roy. Soc.* **222** (1921) 167-226.

- [15] A.F. Bicen and J.H. Whitelaw, "Velocity Characteristics of the Wake of an In-Cylinder Projectile," *Imperial College of Science and Technology Report FS/83/19*, London, England, June 1983.
- [16] R. Heiser and J. A. Schmitt, "Simulations of Special Interior Ballistic Phenomena With and Without Heat Transfer to the Gun Tube Wall," *Proceedings of the Second Army Conference on Applied Mathematics and Computing*, ARO Report, 1984.

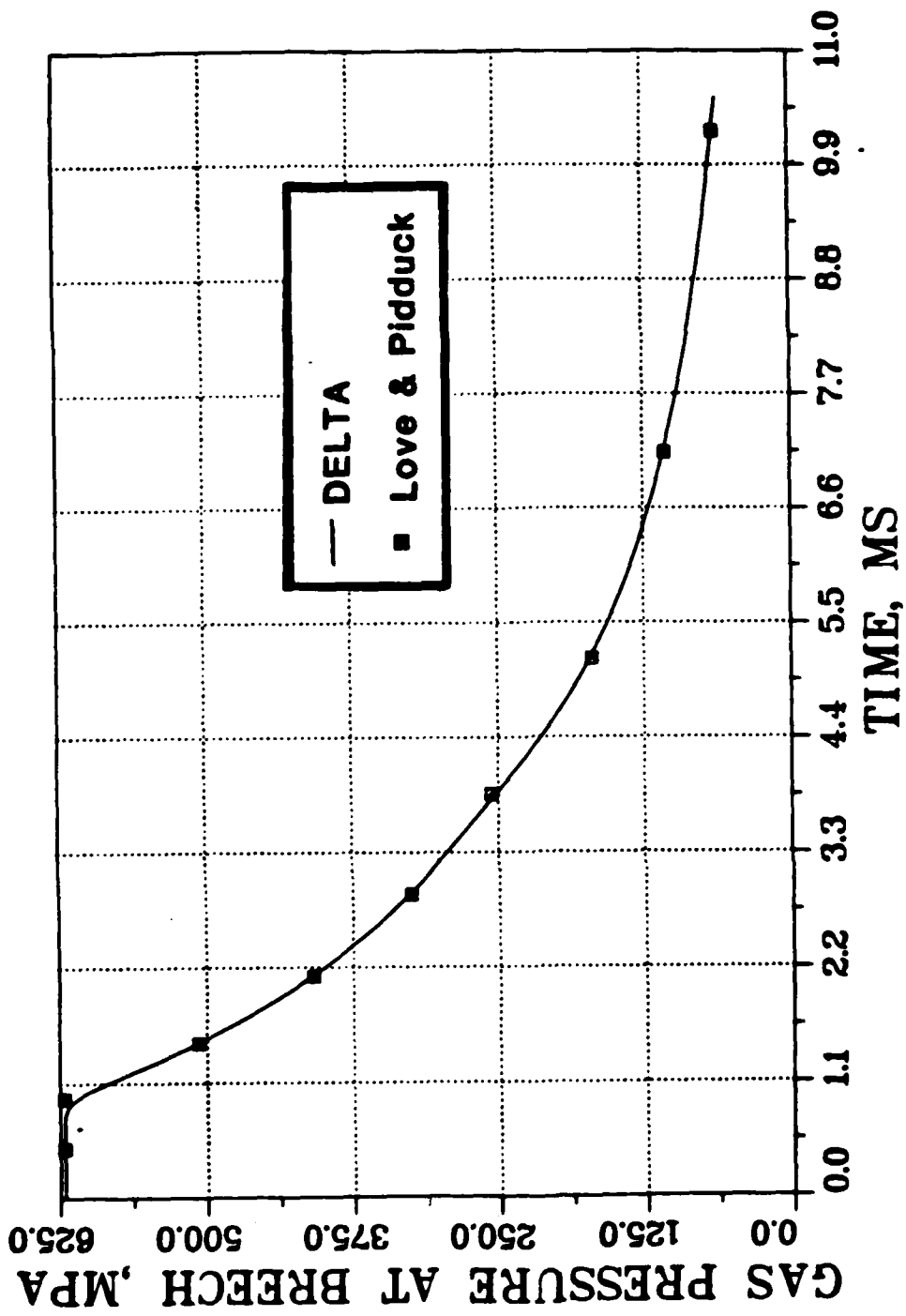


Figure 2. The comparison of the pressure histories at the breach.

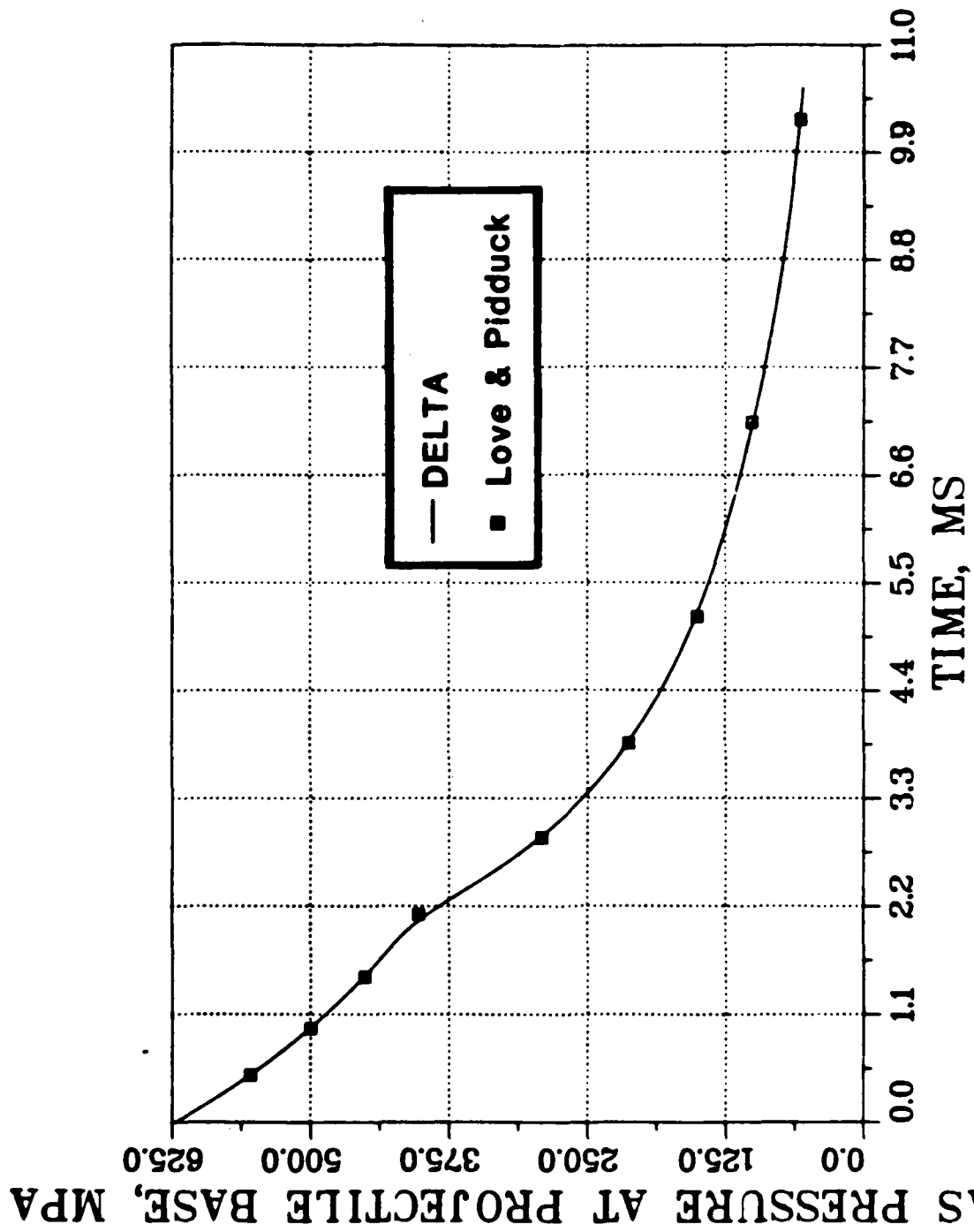


Figure 1. The comparison of the pressure histories at the projectile base.

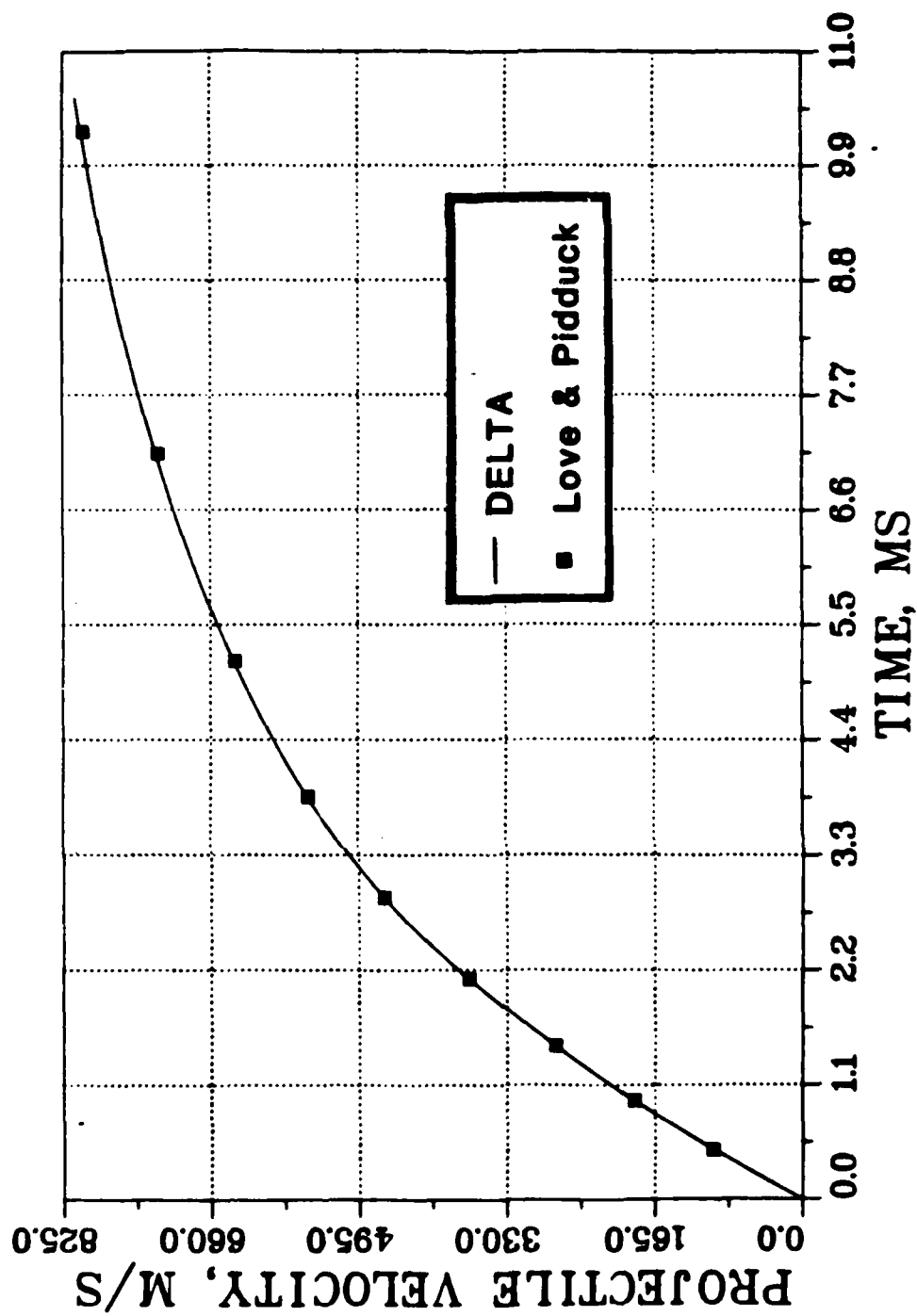


Figure 3. The comparison of the histories of the projectile velocity.

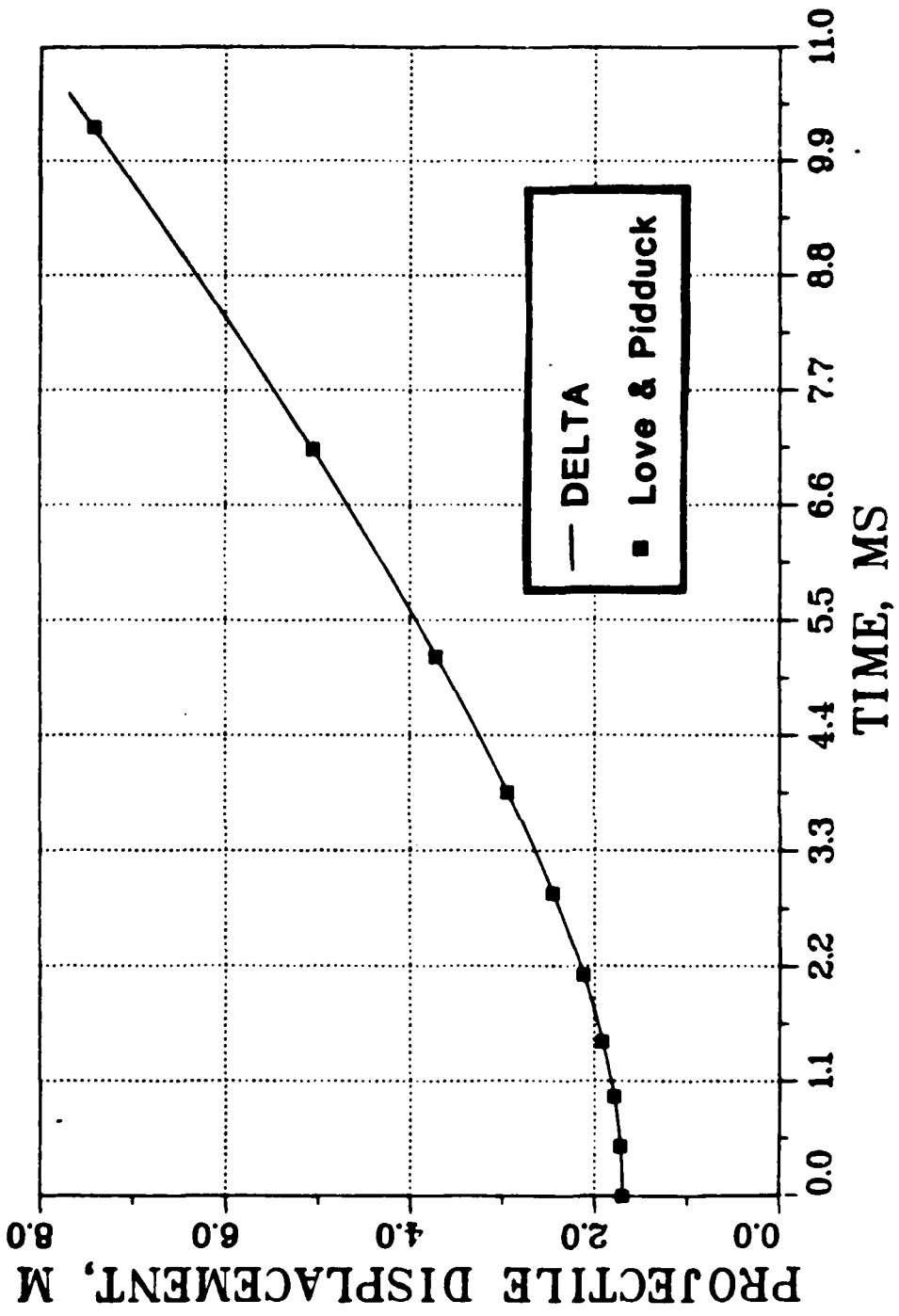


Figure 4. The comparison of the histories of the projectile displacement.

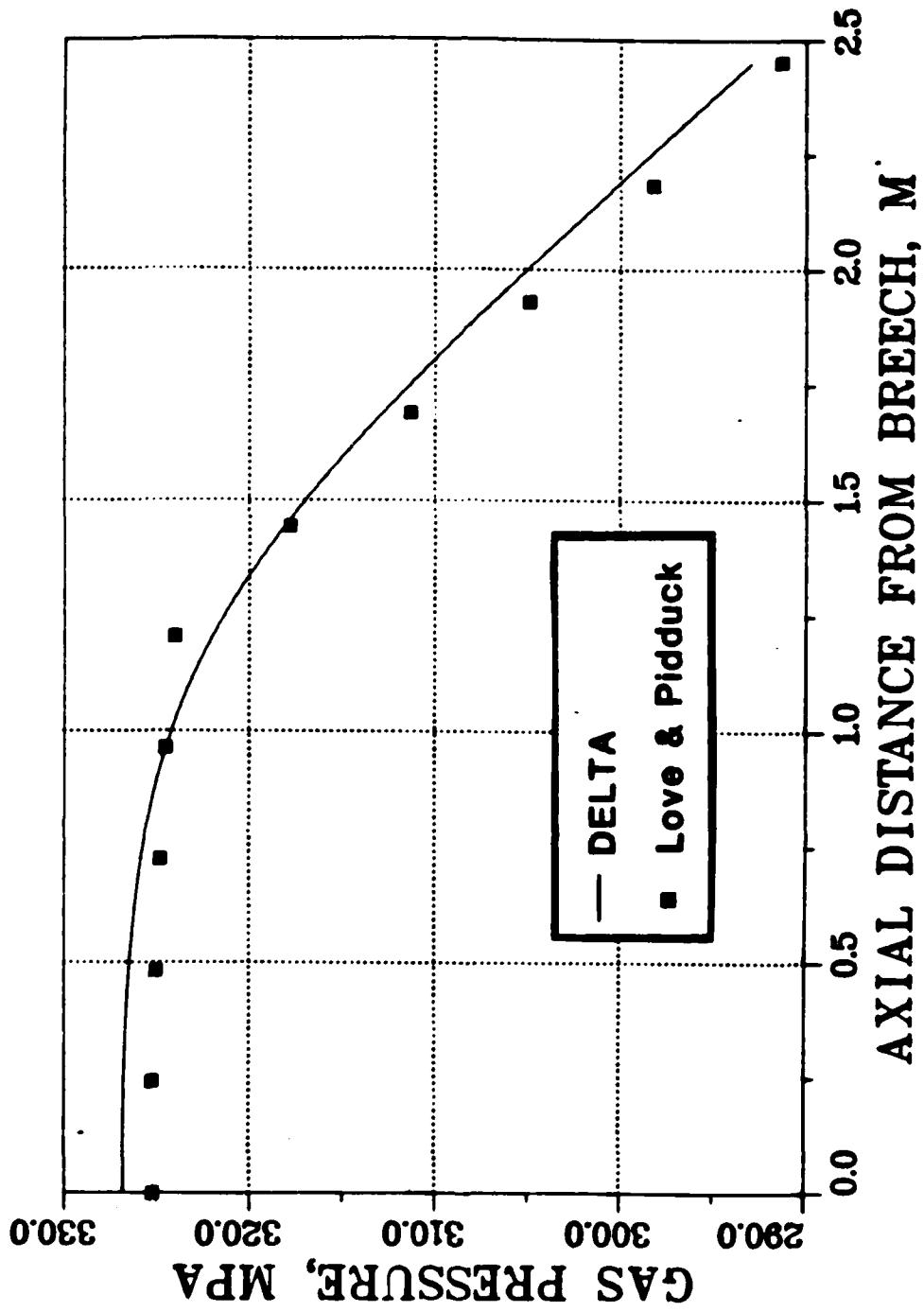


Figure 5. The comparison of the pressure profiles from the breach to the projectile at time 2.898ms.

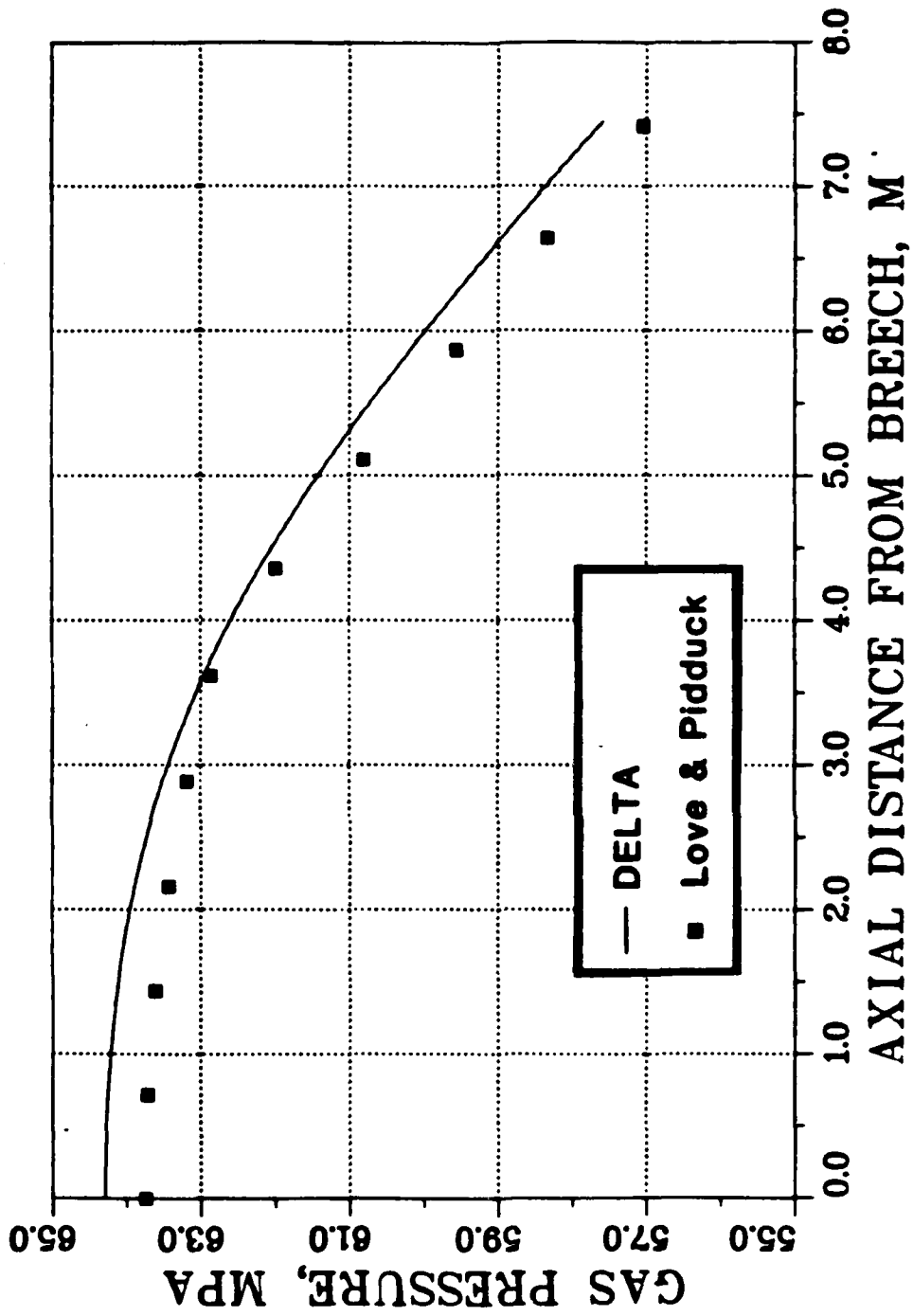


Figure 6. The comparison of the pressure profiles from the breach to the projectile at time 10.23ms.

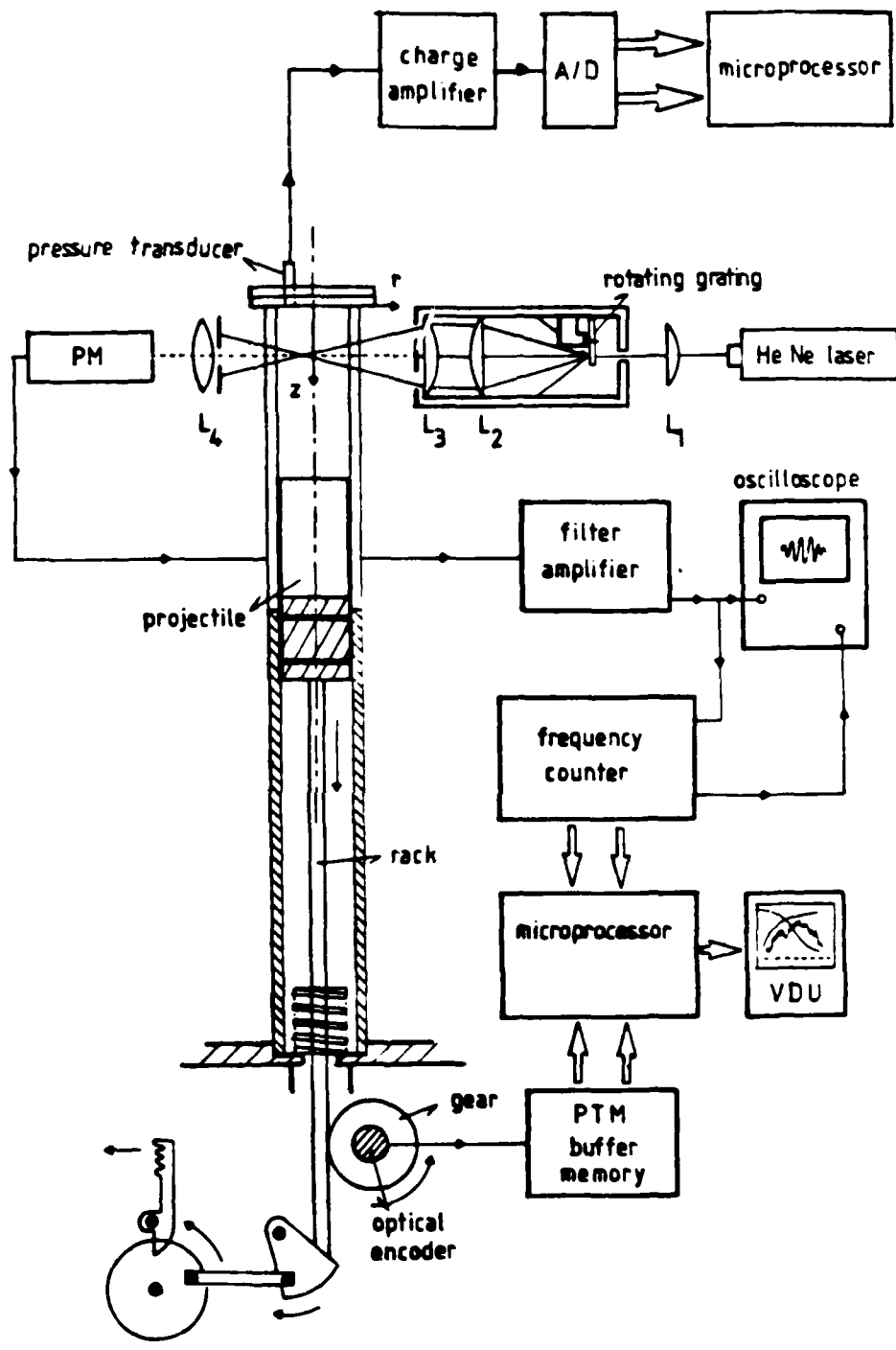


Figure 7. A schematic of the Bicen-Whitelaw experimental apparatus

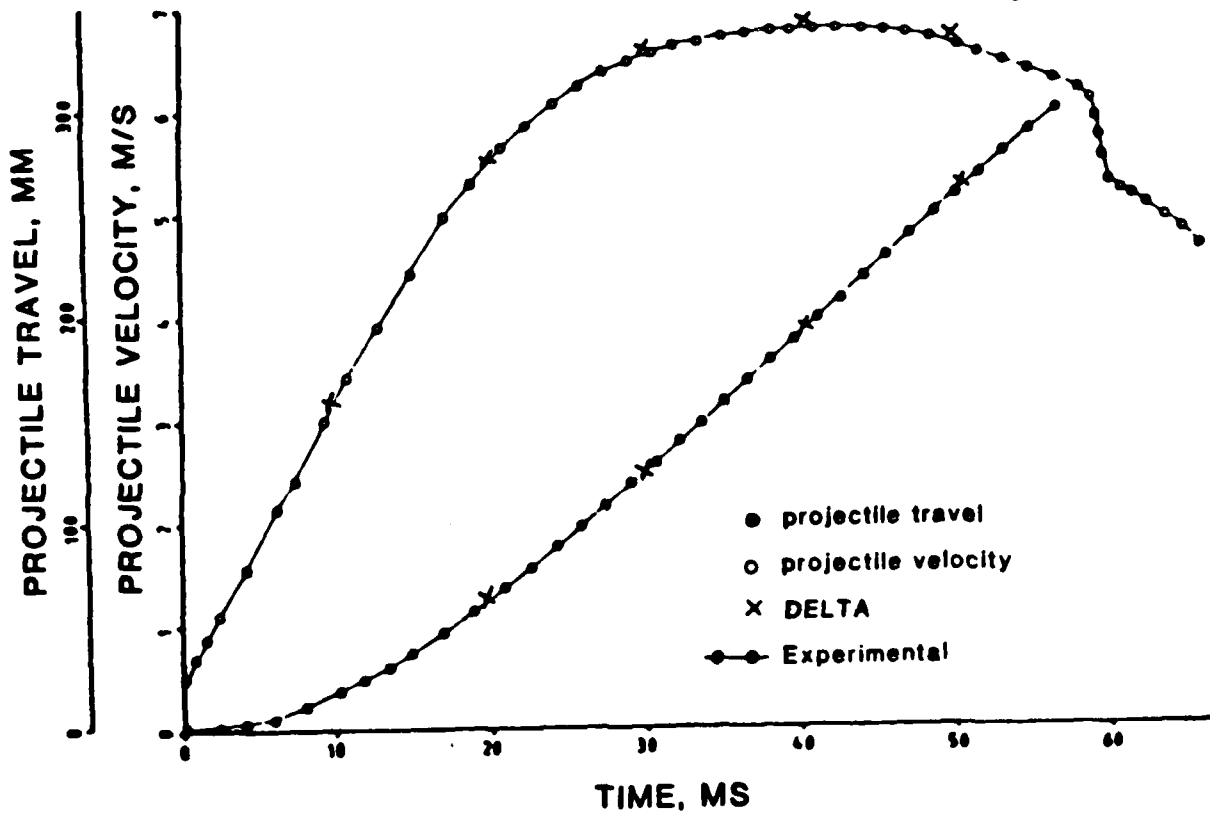


Figure 8. The comparison of the axial velocities and displacements of the projectile.

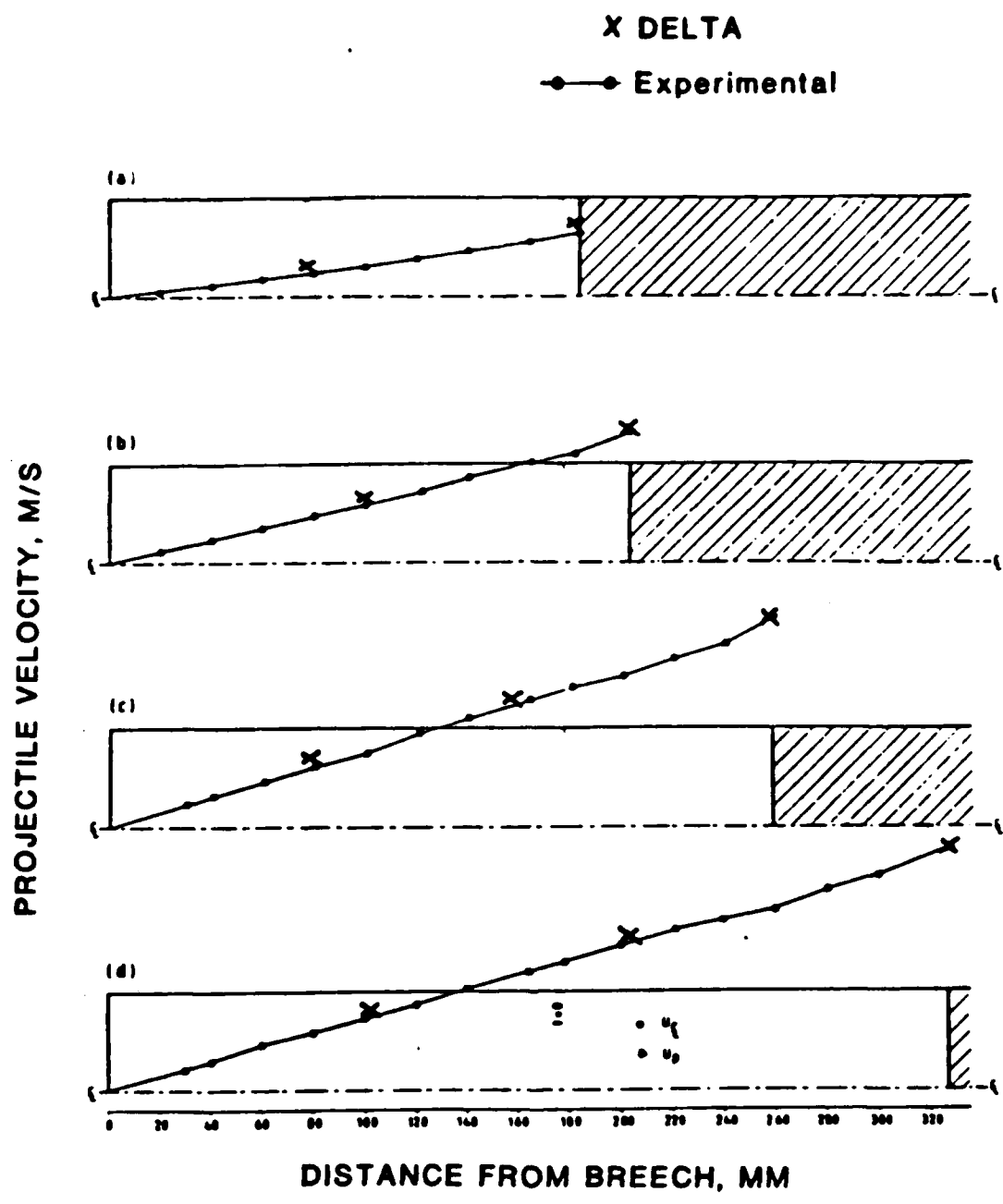


Figure 9. The comparison of the axial velocity profiles along the axis of symmetry at various times:  
 (a) 4.8ms                      (c) 22.8ms  
 (b) 11.6ms                     (d) 33.8ms

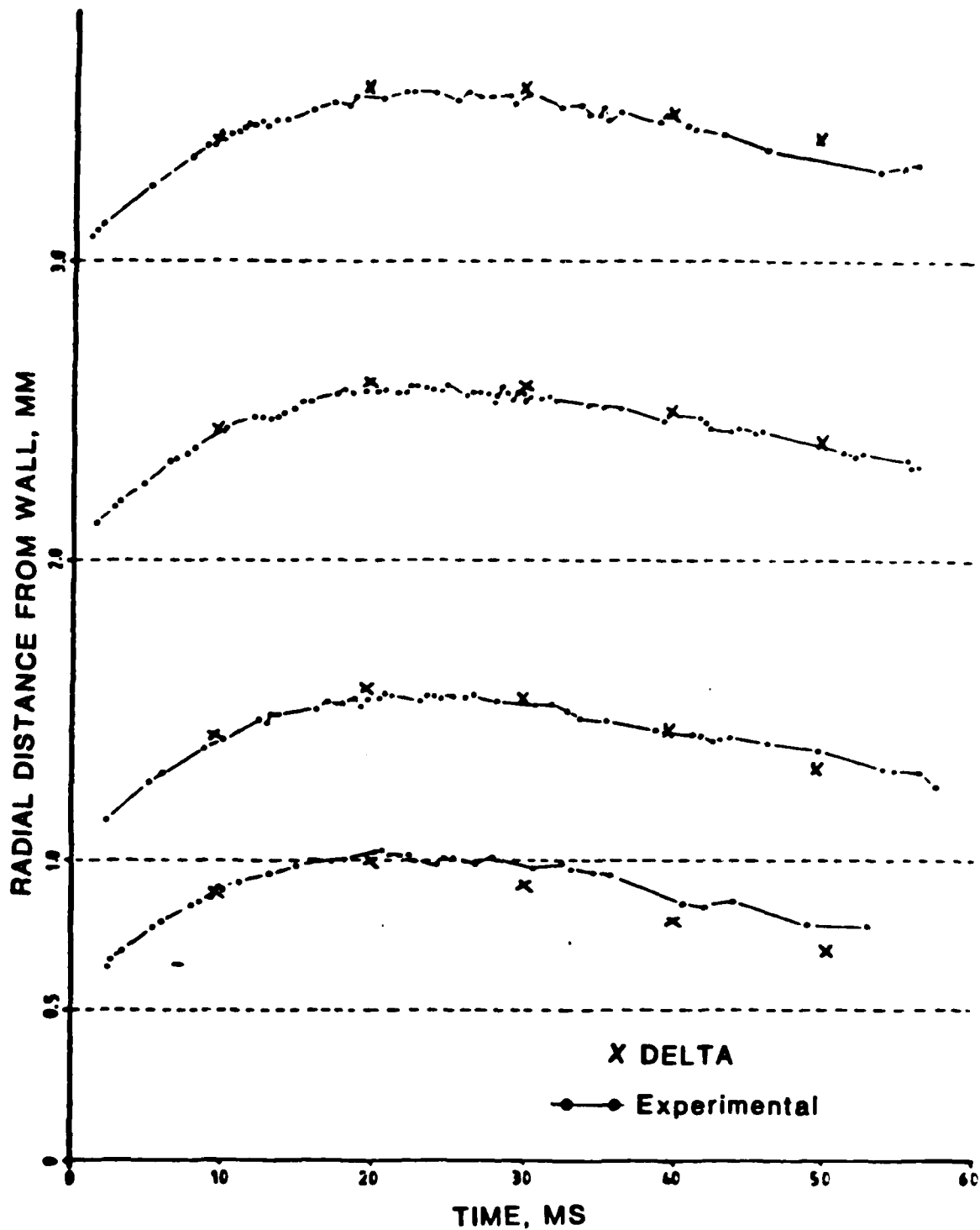


Figure 10. The comparison of the axial velocity histories at 77.6mm from the breech.

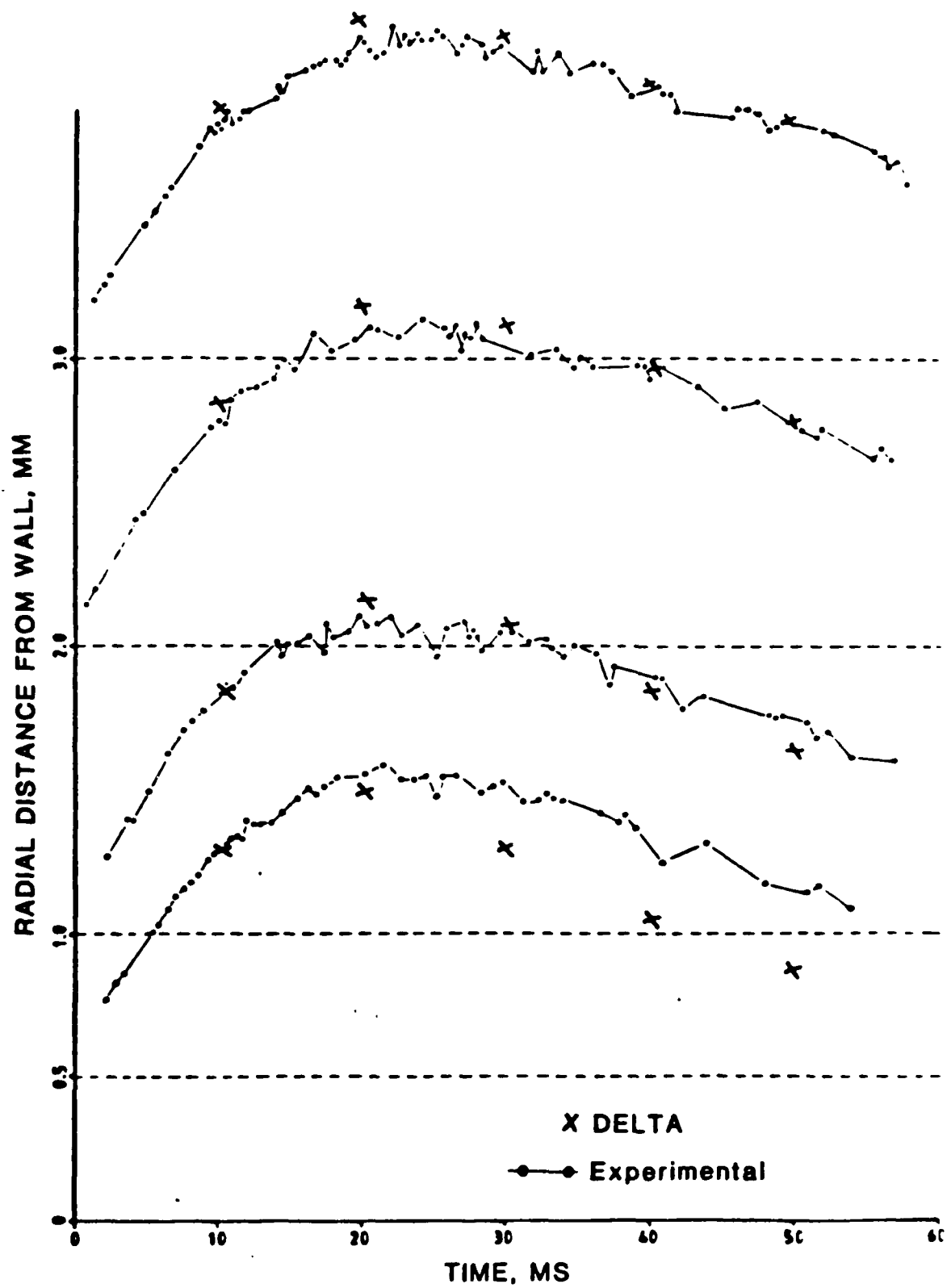


Figure 11. The comparison of the axial velocity histories at 153.4mm from the breech.

DISTRIBUTION LIST

<u>No. of Copies</u>	<u>Organization</u>	<u>No. of Copies</u>	<u>Organization</u>
12	Administrator Defense Technical Info Center ATTN: DTIC-FDAC Cameron Station, Bldg 5 Alexandria, VA 22304-6145	5	Project Manager Cannon Artillery Weapons System, ARDC, AMCCOM ATTN: AMCPM-CW, AMCPM-CWW AMCPM-CWS M. Fisette AMCPM-CWA H. Hassmann AMCPM-CWA-S R. DeKleine Dover, NJ 07801-5001
1	Commander USA Concepts Analysis Agency ATTN: D. Hardison 8120 Woodmont Avenue Bethesda, MD 20014-2797		
1	HQDA/DAMA-ZA Washington, DC 20310-2500	2	Project Manager Munitions Production Base Modernization and Expansion ATTN: AMCPM-PBM, A. Siklosi AMCPM-PBM-E, L. Laibson Dover, NJ 07801-5001
1	HQDA, DAMA-CSM, Washington, DC 20310-2500		
1	HQDA/SARDA Washington, DC 20310-2500		
1	C.I.A. OIR/DB/Standard GE47 HQ Washington, D.C. 20505	3	Project Manager Tank Main Armament System ATTN: AMCPM-TMA, K. Russell AMCPM-TMA-105 AMCPM-TMA-120 Dover, NJ 07801-5001
1	Commander US Army War College ATTN: Library-FF229 Carlisle Barracks, PA 17013	1	Commander US Army Watervliet Arsenal ATTN: SARWV-RD, R. Thierry Watervliet, NY 12189-5001
1	US Army Ballistic Missile Defense Systems Command Advanced Technology Center P. O. Box 1500 Huntsville, AL 35807-3801	1	Commander U.S. Army ARDEC ATTN: SMCAR-MSI Dover, NJ 07801-5001
1	Chairman DOD Explosives Safety Board Room 856-C Hoffman Bldg. 1 2461 Eisenhower Avenue Alexandria, VA 22331-9999	1	Commander U.S. Army ARDEC ATTN: SMCAR-TDC Dover, NJ 07801-5001
1	Commander US Army Materiel Command ATTN: AMCPM-GCM-WF 5001 Eisenhower Avenue Alexandria, VA 22333-5001	4	Commander US Army Armament Munitions and Chemical Command ATTN: AMSMC-IMP-L Rock Island, IL 61299-7300
1	Commander US Army Materiel Command ATTN: AMCDRA-ST 5001 Eisenhower Avenue Alexandria, VA 22333-5001	1	HQDA DAMA-ART-M Washington, DC 20310-2500
1	Commander US Army Materiel Command ATTN: AMCDE-DW 5001 Eisenhower Avenue Alexandria, VA 22333-5001	1	Commander US Army AMCCOM ARDEC CCA ATTN: SMCAR-CCB-TL Benet Weapons Laboratory Watervliet, NY 12189-4050

### DISTRIBUTION LIST

<u>No. of Copies</u>	<u>Organization</u>	<u>No. of Copies</u>	<u>Organization</u>
3	Commander US Army ARDEC ATTN: SMCAR-MSI SMCAR-TDC SMCAR-LC LTC N. Barron Dover, NJ 07801-5001	1	Commander US Army Communications - Electronics Command ATTN: AMSEL-ED Fort Monmouth, NJ 07703-5301
7	Commander US Army ARDEC ATTN: SMCAR-LCA A. Beardell D. Downs S. Einstein S. Westley S. Bernstein C. Roller J. Rutkowski Dover, NJ 07801-5001	1	Commander CECOM R&D Technical Library ATTN: AMSEL-M-L (Report Section) B.2700 Fort Monmouth, NJ 07703-5000
3	Commander US Army ARDEC ATTN: SMCAR-LCB-I D. Spring SMCAR-LCE SMCAR-LCM-E S. Kaplowitz Dover, NJ 07801-5001	1	Commander US Army Harry Diamond Lab. ATTN: DELHD-TA-L 2800 Powder Mill Road Adelphi, MD 20783-1145
4	Commander US Army ARDEC ATTN: SMCAR-LCS SMCAR-LCU-CT E. Barrieres R. Davitt SMCAR-LCU-CV C. Mandala Dover, NJ 07801-5001	1	Commander US Army Missile Command ATTN: AMSMI-RX M.W. Thauer Redstone Arsenal, AL 35898-5249
3	Commander US Army ARDEC ATTN: SMCAR-LCW-A M. Salsbury SMCAR-SCA L. Stiefel B. Brodman Dover, NJ 07801-5001	1	Commander US Army Missile and Space Intelligence Center ATTN: AIAMS-YDL Redstone Arsenal, AL 35898-5500
1	Commander US Army ARDEC ATTN: AMSAV-ES 4300 Goodfellow Blvd. St. Louis, MO 63120-1798	1	Commander US Army Missile Command Research, Development, and Engineering Center ATTN: AMSMI-RD Redstone Arsenal, AL 35898-5245
1	Director US Army Aviation Research and Technology Activity Ames Research Center Moffett Field, CA 94035-1099	1	Commandant US Army Aviation School ATTN: Aviation Agency Fort Rucker, AL 36360
		1	Commander US Army Tank Automotive Command ATTN: AMSTA-TSL Warren, MI 48397-5000
		1	Commander US Army Tank Automotive Command ATTN: AMSTA-CG Warren, MI 48397-5000

## DISTRIBUTION LIST

<u>No. of Copies</u>	<u>Organization</u>	<u>No. of Copies</u>	<u>Organization</u>
1	Project Manager Improved TOW Vehicle ATTN: AMCPM-ITV US Army Tank Automotive Command Warren, MI 48397-5000	1	Commander US Army Logistics Mgmt Ctr Defense Logistics Studies Fort Lee, VA 23801
2	Program Manager MI Abrams Tank System ATTN: AMCPM-GMC-SA, T. Dean Warren, MI 48092-2498	1	Commandant US Army Infantry School ATTN: ATSH-CD-CS-OR Fort Benning, GA 31905-5400
1	Project Manager Fighting Vehicle Systems ATTN: AMCPM-FVS Warren, MI 48092-2498	1	Commandant US Army Command and General Staff College Fort Leavenworth, KS 66027
1	President US Army Armor & Engineer Board ATTN: ATZK-AD-S Fort Knox, KY 40121-5200	1	Commandant US Army Special Warfare School ATTN: Rev & Tng Lit Div Fort Bragg, NC 28307
1	Project Manager M-60 Tank Development ATTN: AMCPM-M60TD Warren, MI 48092-2498	3	Commander Radford Army Ammunition Plant ATTN: SMCRA-QA/HI LIB Radford, VA 24141-0298
1	Director US Army TRADOC Systems Analysis Activity ATTN: ATOR-TSL White Sands Missile Range, NM 88002	1	Commander US Army Foreign Science & Technology Center ATTN: AMXST-MC-3 220 Seventh Street, NE Charlottesville, VA 22901-5396
1	Commander US Army Training & Doctrine Command ATTN: ATCD-MA/ MAJ Williams Fort Monroe, VA 23651	2	Commandant US Army Field Artillery Center & School ATTN: ATSF-CO-MW, B. Willis Ft. Sill, OK 73503-5600
2	Commander US Army Materials and Mechanics Research Center ATTN: AMXMR-ATL Tech Library Watertown, MA 02172	1	Commander US Army Development and Employment Agency ATTN: MODE-ORO Fort Lewis, WA 98433-5099
1	Commander US Army Research Office ATTN: Tech Library P. O. Box 12211 Research Triangle Park, NC 27709-2211	1	Office of Naval Research ATTN: Code 473, R. S. Miller 800 N. Quincy Street Arlington, VA 22217-9999
1	Commander US Army Belvoir Research and Development Center ATTN: STRBE-WC Fort Belvoir, VA 22060-5606	3	Commandant US Army Armor School ATTN: ATZK-CD-MS M. Falkovitch Armor Agency Fort Knox, KY 40121-5215

## DISTRIBUTION LIST

<u>No. of Copies</u>	<u>Organization</u>	<u>No. of Copies</u>	<u>Organization</u>
2	<b>Commander</b> Naval Sea Systems Command ATTN: SEA 62R SEA 64 Washington, DC 20362-5101	2	<b>Superintendent</b> Naval Postgraduate School Dept. of Mech. Engineering Monterey, CA 93943-5100
1	<b>Commander</b> Naval Air Systems Command ATTN: AIR-954-Tech Lib Washington, DC 20360	1	<b>Program Manager</b> AFOSR Directorate of Aerospace Sciences ATTN: L. H. Caveny Bolling AFB, DC 20332-0001
1	<b>Assistant Secretary of the</b> Navy (R, E, and S) ATTN: R. Reichenbach Room 5E787 Pentagon Bldg. Washington, DC 20350	5	<b>Commander</b> Naval Ordnance Station ATTN: P. L. Stang L. Torreyson T. C. Smith D. Brooks Tech Library Indian Head, MD 20640-5000
1	<b>Naval Research Lab</b> Tech Library Washington, DC 20375	1	<b>AFSC/SDOA</b> Andrews AFB, MD 20334
5	<b>Commander</b> Naval Surface Weapons Center ATTN: Code G33, J. L. East W. Burrell J. Johndrow Code G23, D. McClure Code DX-21 Tech Lib Dahlgren, VA 22448-5000	3	<b>AFRPL/DY, Stop 24</b> ATTN: J. Levine/DYCR R. Corley/DYC D. Williams/DYCC Edwards AFB, CA 93523-5000
2	<b>Comander</b> US Naval Surface Weapons Center ATTN: J. P. Consaga C. Gotzmer Indian Head, MD 20640-5000	1	<b>AFRPL/TSTL (Tech Library)</b> Stop 24 Edwards AFB, CA 93523-5000
4	<b>Commander</b> Naval Surface Weapons Center ATTN: S. Jacobs/Code 240 Code 730 K. Kim/Code R-13 R. Bernecker Silver Spring, MD 20903-5000	1	<b>AFATL/DLYV</b> Eglin AFB, FL 32542-5000
4	<b>Commander</b> Naval Surface Weapons Center ATTN: S. Jacobs/Code 240 Code 730 K. Kim/Code R-13 R. Bernecker Silver Spring, MD 20903-5000	1	<b>AFATL/DLXP</b> Eglin AFB, FL 32542-5000
2	<b>Commanding Officer</b> Naval Underwater Systems Center Energy Conversion Dept. ATTN: CODE 5B331, R. S. Lazar Tech Lib Newport, RI 02840	1	<b>AFATL/DLJE</b> Eglin AFB, FL 32542-5000
2	<b>Commanding Officer</b> Naval Underwater Systems Center Energy Conversion Dept. ATTN: CODE 5B331, R. S. Lazar Tech Lib Newport, RI 02840	1	<b>AFATL/DOIL</b> ATTN: (Tech Info Center) Eglin AFB, FL 32542-5438
4	<b>Commander</b> Naval Weapons Center ATTN: Code 388, R. L. Derr C. F. Price T. Boggs Info. Sci. Div. China Lake, CA 93555-6001	1	<b>NASA/Lyndon B. Johnson Space                      Center</b> ATTN: NHS-22, Library Section Houston, TX 77054
		1	<b>AFELM, The Rand Corporation</b> ATTN: Library D 1700 Main Street Santa Monica CA 90401-3297

## DISTRIBUTION LIST

<u>No. of Copies</u>	<u>Organization</u>	<u>No. of Copies</u>	<u>Organization</u>
1	General Applied Sciences Lab ATTN: J. Erdos Merrick & Stewart Avenues Westbury Long Isl, NY 11590	1	Hercules, Inc. Radford Army Ammunition Plant ATTN: J. Pierce Radford, VA 24141-0299
2	AAI Corporation ATTN: J. Hebert J. Frankle D. Cleveland P. O. Box 6767 Baltimore, MD 21204	1	Honeywell, Inc. - MN64 2200 Defense Systems Division ATTN: C. Hargreaves 6110 Blue Circle Drive Minnetonka MN 55436
1	Aerojet Ordnance Company ATTN: D. Thatcher 2521 Michelle Drive Tustin, CA 92680-7014	1	Lawrence Livermore National Laboratory ATTN: L-355, A. Buckingham M. Finger P. O. Box 808 Livermore, CA 94550-0622
1	Aerojet Solid Propulsion Co. ATTN: P. Micheli Sacramento, CA 95813	1	Lawrence Livermore National Laboratory ATTN: L-324/M. Constantino P. O. Box 808 Livermore, CA 94550-0622
1	Atlantic Research Corporation ATTN: M. K. King 5390 Cheorokee Avenue Alexandria, VA 22312-2302	1	Olin Corporation Badger Army Ammunition Plant ATTN: R. J. Thiede Baraboo, WI 53913
1	AVCO Everett Rsch Lab ATTN: D. Stickler 2385 Revere Beach Parkway Everett, MA 02149-5936	1	Olin Corporation Smokeless Powder Operations ATTN: D. C. Mann P.O. Box 222 St. Marks, FL 32355-0222
2	Calspan Corporation ATTN: C. Morphy P. O. Box 400 Buffalo, NY 14225-0400	1	Paul Gough Associates, Inc. ATTN: P. S. Gough P. O. Box 1614, 1048 South St. Portsmouth, NH 03801-1614
1	General Electric Company Armament Systems Dept. ATTN: M. J. Bulman, Room 1311 128 Lakeside Avenue Burlington, VT 05401-4985	1	Physics International Company ATTN: Library H. Wayne Wampler 2700 Merced Street San Leandro, CA 94577-5602
1	IITRI ATTN: M. J. Klein 10 W. 35th Street Chicago, IL 60616-3799	1	Princeton Combustion Research Lab., Inc. ATTN: M. Summerfield 475 US Highway One Monmouth Junction, NJ 08852-9650
1	Hercules Inc. Allegheny Ballistics Laboratory ATTN: R. B. Miller P. O. Box 210 Cumberland, MD 21501-0210	1	Rockwell International Rocketdyne Division ATTN: BA08 J. E. Flanagan J. Gray 6633 Canoga Avenue Canoga Park, CA 91303-2703
1	Hercules, Inc. Bacchus Works ATTN: K. P. McCarty P. O. Box 98 Magna, UT 84044-0098	2	

## DISTRIBUTION LIST

<u>No. of Copies</u>	<u>Organization</u>	<u>No. of Copies</u>	<u>Organization</u>
1	Science Applications, Inc. ATTN: R. B. Edelman 23146 Cumorah Crest Drive Woodland Hills, CA 91364-3710	1	University of Illinois Dept of Mech/Indust Engr ATTN: H. Krier 144 MEB; 1206 N. Green St. Urbana, IL 61801-2978
3	Thiokol Corporation Huntsville Division ATTN: D. Flanigan R. Glick Tech Library Huntsville, AL 35807	1	University of Massachusetts Dept. of Mech. Engineering ATTN: K. Jakus Amherst, MA 01002-0014
2	Thiokol Corporation Elkton Division ATTN: R. Biddle Tech Lib. P. O. Box 241 Elkton, MD 21921-0241	1	University of Minnesota Dept. of Mech. Engineering ATTN: E. Fletcher Minneapolis, MN 55414-3368
2	United Technologies Chemical Systems Division ATTN: R. Brown Tech Library P. O. Box 358 Sunnyvale, CA 94086-9998	1	Case Western Reserve University Division of Aerospace Sciences ATTN: J. Tien Cleveland, OH 44135
1	Veritay Technology, Inc. ATTN: E. Fisher 4845 Millersport Hwy. P. O. Box 305 East Amherst, NY 14051-0305	3	Georgia Institute of Tech School of Aerospace Eng. ATTN: B. T. Zinn E. Price W. C. Strahle Atlanta, GA 30332
1	Universal Propulsion Company ATTN: H. J. McSpadden Black Canyon Stage 1 Box 1140 Phoenix, AZ 85029	1	Institute of Gas Technology ATTN: D. Gidaspow 3424 S. State Street Chicago, IL 60616-3896
1	Battelle Memorial Institute ATTN: Tech Library 505 King Avenue Columbus, OH 43201-2693	1	Johns Hopkins University Applied Physics Laboratory Chemical Propulsion Information Agency ATTN: T. Christian Johns Hopkins Road Laurel, MD 20707-0690
1	Brigham Young University Dept. of Chemical Engineering ATTN: M. Beckstead Provo, UT 84601	1	Massachusetts Institute of Technology Dept of Mechanical Engineering ATTN: T. Toong 77 Massachusetts Avenue Cambridge, MA 02139-4307
1	California Institute of Tech 204 Karman Lab Main Stop 301-46 ATTN: F. E. C. Culick 1201 E. California Street Pasadena, CA 91109	1	G. M. Faeth Pennsylvania State University Applied Research Laboratory University Park, PA 16802-7501
1	California Institute of Tech Jet Propulsion Laboratory ATTN: L. D. Strand 4800 Oak Grove Drive Pasadena, CA 91109-8099	1	Pennsylvania State University Dept. of Mech. Engineering ATTN: K. Kuo University Park, PA 16802-7501

DISTRIBUTION LIST

<u>No. of Copies</u>	<u>Organization</u>	<u>No. of Copies</u>	<u>Organization</u>
1	Purdue University School of Mechanical Engineering ATTN: J. R. Osborn TSPC Chaffee Hall West Lafayette, IN 47907-1199	Cdr, USATECOM ATTN: AMSTE-SI-F AMSTE-CM-F, L. Nealley	
1	SRI International Propulsion Sciences Division ATTN: Tech Library 333 Ravenswood Avenue Menlo Park, CA 94025-3493	Cdr, CSTA ATTN: STECS-AS-H, R. Hendricksen	
1	Rensselaer Polytechnic Inst. Department of Mathematics Troy, NY 12181	Cdr, CRDC, AMCCOM ATTN: SMCCR-RSP-A SMCCR-MU SMCCR-SPS-IL	
2	Director Los Alamos Scientific Lab ATTN: T3, D. Butler M. Division, B. Craig P. O. Box 1663 Los Alamos, NM 87544		
1	Stevens Institute of Technology Davidson Laboratory ATTN: R. McAlevy, III Castle Point Station Hoboken, NJ 07030-5907		
1	Rutgers University Dept. of Mechanical and Aerospace Engineering ATTN: S. Temkin University Heights Campus New Brunswick, NJ 08903		
1	University of Southern California Mechanical Engineering Dept. ATTN: OHE200, M. Gerstein Los Angeles, CA 90089-5199		
2	University of Utah Dept. of Chemical Engineering ATTN: A. Baer G. Flandro Salt Lake City, UT 84112-1194		
1	Washington State University Dept. of Mech. Engineering ATTN: C. T. Crowe Pullman, WA 99163-5201		

Aberdeen Proving Ground

Dir, USAMSA  
ATTN: AMXSY-D  
AMXSY-MP, H. Cohen

USER EVALUATION SHEET/CHANGE OF ADDRESS

This Laboratory undertakes a continuing effort to improve the quality of the reports it publishes. Your comments/answers to the items/questions below will aid us in our efforts.

1. BRL Report Number \_\_\_\_\_ Date of Report \_\_\_\_\_

2. Date Report Received \_\_\_\_\_

3. Does this report satisfy a need? (Comment on purpose, related project, or other area of interest for which the report will be used.) \_\_\_\_\_  
\_\_\_\_\_  
\_\_\_\_\_

4. How specifically, is the report being used? (Information source, design data, procedure, source of ideas, etc.) \_\_\_\_\_  
\_\_\_\_\_  
\_\_\_\_\_

5. Has the information in this report led to any quantitative savings as far as man-hours or dollars saved, operating costs avoided or efficiencies achieved, etc? If so, please elaborate. \_\_\_\_\_  
\_\_\_\_\_  
\_\_\_\_\_

6. General Comments. What do you think should be changed to improve future reports? (Indicate changes to organization, technical content, format, etc.) \_\_\_\_\_  
\_\_\_\_\_  
\_\_\_\_\_

CURRENT ADDRESS  
Name \_\_\_\_\_  
Organization \_\_\_\_\_  
Address \_\_\_\_\_  
City, State, Zip \_\_\_\_\_

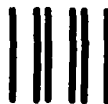
7. If indicating a Change of Address or Address Correction, please provide the New or Correct Address in Block 6 above and the Old or Incorrect address below.

OLD ADDRESS  
Name \_\_\_\_\_  
Organization \_\_\_\_\_  
Address \_\_\_\_\_  
City, State, Zip \_\_\_\_\_

(Remove this sheet, fold as indicated, staple or tape closed, and mail.)

FOLD HERE

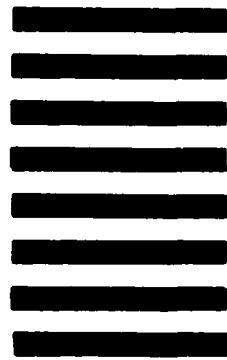
Director  
US Army Ballistic Research Laboratory  
ATTN: DRXBR-OD-ST  
Aberdeen Proving Ground, MD 21005-5066



NO POSTAGE  
NECESSARY  
IF MAILED  
IN THE  
UNITED STATES

OFFICIAL BUSINESS  
PENALTY FOR PRIVATE USE, \$300

**BUSINESS REPLY MAIL**  
FIRST CLASS PERMIT NO 12062 WASHINGTON, DC  
POSTAGE WILL BE PAID BY DEPARTMENT OF THE ARMY



Director  
US Army Ballistic Research Laboratory  
ATTN: DRXBR-OD-ST  
Aberdeen Proving Ground, MD 21005-9989

FOLD HERE

END

FEB.

1988

DTIC